IDENTIFICATION AND SEGMENTATION OF THE CENTRAL SULCUS FROM HUMAN BRAIN MR IMAGES

ZUO WEI
(B.ENG., HUST)

A THESIS SUBMITTED

FOR THE DEGREE OF MASTER OF SCIENCE

SCHOOL OF COMPUTING

NATIONAL UNIVERSITY OF SINGAPORE

2004

Acknowledgements

First of all, I feel deeply indebted to my supervisors Prof. Nowinski Wieslaw, Dr. Hu Qingmao and Associate Prof. Loe Kia Fock, without whom the completion of this thesis could not have been possible. I would like to take this opportunity to express my deepest appreciation and sincere gratitude to them for their inspiring guidance, advice and kindly patience.

I am grateful to Dr. Aamer Aziz, Mr. Xiao Pengdong, Mr. Huang Su, Mr. Lin Chunshu and all my colleagues in the Biomedical Imaging Lab of the Institute for Infocomm Research (I2R) for their valuable instruction and generous assistance, which have been a great source of help in the completion of this thesis.

I am also grateful to Wang Zhenlan, Lu Yiping, Wang Zhengjia, Qian Wenlong, Gao Chunping, Li Yang and Kang Yulin, who have been always encouraging, supporting and helping me during my postgraduate study.

I gratefully acknowledge the financial support from the Biomedical Research Council, the Agency for Science, Technology and Research and National University of Singapore for the duration of this project. Otherwise, I would not be able to undertake my further study on this project in I2R.

Finally, I want to show my deep appreciation to my family and girl friend for their constant caring and support throughout my life. There are many others who have assisted me in various ways during this project. I gratefully acknowledge their help.

Table of Content

List of Figures

List of Table

Summary

The purpose of this dissertation is to develop a fast knowledge-driven algorithm to identify and segment the central sulcus (CS) from human brain magnetic resonance (MR) volumetric images automatically. The CS is an important landmark in the human brain since it demarcates the primary motor and somatosensory areas of the cortex.

The dataset is reformatted first along the anterior commissure (AC) and posterior commissure (PC) plane. Then, the skull is removed and the mask of the brain tissues is obtained through classification and morphological processing. The three-dimensional (3D) region within two coronal planes passing through the AC and PC is defined as the region of interest (ROI) to search for all sulci. The CS is the sulcus with the largest volume within the ROI. Together with the sulci, grey matter (GM) is included for region growing in order to deal with the partial volume effect. Most GM is later removed through skeletonization while some GM component is kept to maintain the connectivity of the sulci. The cerebrospinal fluid (CSF) voxels based on thresholding which are connected to the skeleton are added to the skeleton to yield the final CS. An algorithm is proposed to remove over-segmentation due to leakage through limiting the increase in number of sulcal voxels of neighboring axial slices. With the help of this algorithm and a 3D boundary look-up table, over-segmentation of sulci is controlled. The algorithm has been tested against 18 T1-weighted phantom datasets with different noise levels (0-9%) and inhomogeneity levels (0-40%) and 4

patient-specific datasets. The CSs in 16 out of 18 phantom datasets and all 4 patient-specific datasets were identified and segmented.

The main advantage of our approach is that it is fully automatic compared to previous approaches and can deal with the partial volume effect by growing GM together with sulci and skeletonization. It is also robust to the noise and inhomogeneity. The combination of anatomical knowledge and the image processing techniques are the keys to resolving the problems. The 3D representation (maximum sulcal volume within the ROI) proves to be an efficient way to present the sulci.

Chapter 1

Introduction

1.1 Background

1.1.1 MRI Technology

Magnetic resonance imaging (MRI) has become the primary technique in the routine diagnosis of many disease processes, replacing and sometimes surpassing computed tomography (CT), (Altshuler et al., 2000 and Hauser et al., 2000). MRI has particular advantages in that it is non-invasive, using non-ionising radiation, and has a high soft-tissue resolution and discrimination in any imaging plane.

The advantages of MRI include: excellent brain tissue contrast, multi-planar imaging, acquisition in any orientation, sensitivity to blood flow, lack of ionizing radiation, indication of structure, function, vasculature, pathology and so on. There are a large number of pulse sequences, including T1-weighted (spin lattice relaxation), T2-weighted (spin spin relaxation), SPGR, PD-weighted.

Since the resultant MR image is based on multiple tissue parameters and can modify tissue contrast, MRI technology is suitable for imaging the human brain.

1.1.2 Human Brain

The study of the human brain, especially the cortex, is challenging due to its highly complex, convoluted folding pattern. Ridges of the folds, called gyri, and the spaces

between the folds, called sulci, define location on the cortical surface and provide a parcellation of the cortex into functionally distinct areas. The gyri and sulci are depicted in **Fig 1.1**:

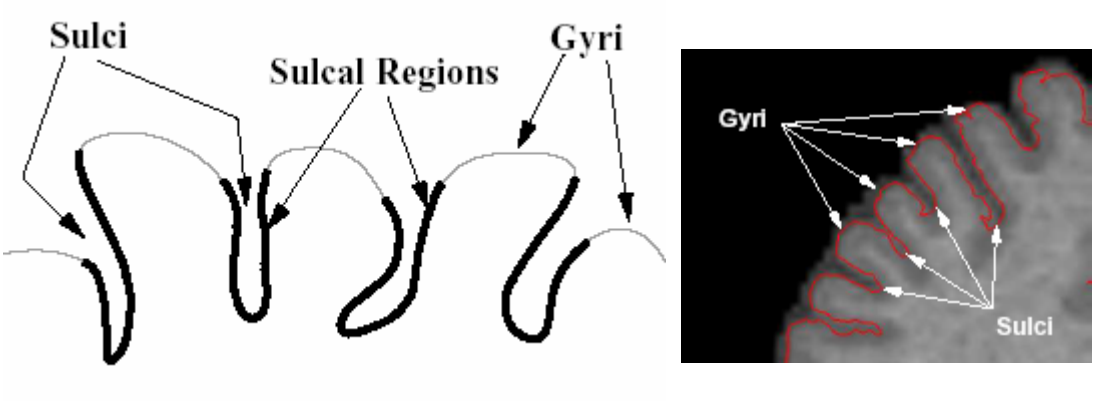

(a) (b)

Fig 1.1 Gyri and sulci depicted in (a) schematic drawing, (b) MR image.

Geometrically, the cerebral cortex is a thin folded sheet of grey matter (GM) that lies inside the cerebrospinal fluid (CSF) and outside the white matter (WM) of the human brain. **Fig 1.2** shows the different components (CSF, GM, WM) in the sulci and gyri:

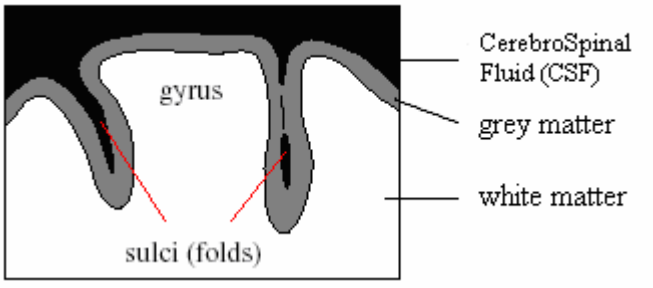

Fig 1.2 The different components (CSF, GM, WM) in the sulci and gyri.

Fig 1.3 shows the segmentation results of the 3 components: (a) WM, (b) GM and (c) CSF.

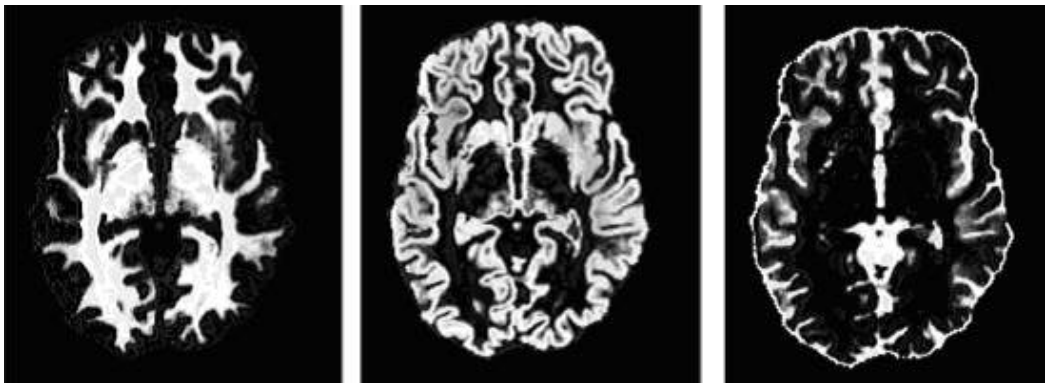

(a) (b) (c)

Fig 1.3 Segmentation of different components: (a) WM, (b) GM, (c) CSF.

1.1.3 Central Sulcus (CS)

The brain is divided into various lobes by fissures. One of the prominent fissures is the central sulcus (CS). It separates the parietal from the frontal lobes. **Fig 1.4** shows the location of the CS:

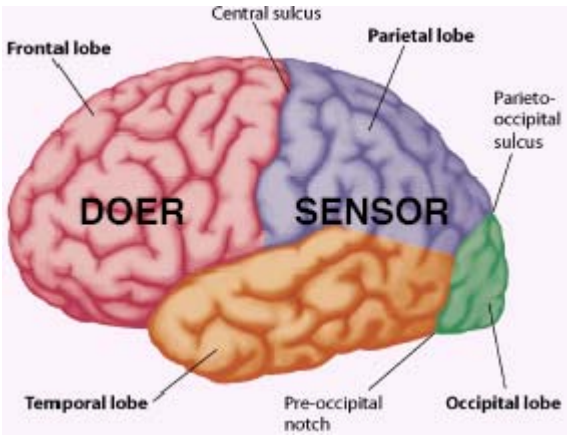

Fig 1.4 The location of the CS and frontal lobe.

Anatomy:

The CS starts in or near the superomedial border slightly behind the midpoint between the frontal and occipital poles (Naidich 1991, Naidich and Brightbill 1996). It runs sinuously downwards and forwards for about 8 to 10 cm to end slightly above the posterior ramus of the lateral sulcus, from which it is always separated by an arched gyrus. Its general direction makes an angle of about 70 degrees with the median plane. It demarcates the primary motor and somatosensory areas of the cortex.

When the sulcus is opened up, its opposed walls are seen to be marked by small gyri, which alternate like gears in a mesh, hence termed *interlocking gyri.* About the middle of the sulcus its walls are usually connected by a transverse gyrus which is due to the mode of development of the central sulcus. When it appears in the sixth month, it is in the superior and inferior parts, at first separated by a transverse gyrus connecting the precentral to postcentral gyrus, shown in **Fig 1.5**. The two occasionally remain separate but usually coalesce, the transverse gyrus being buried as the *deep transitional gyrus.*

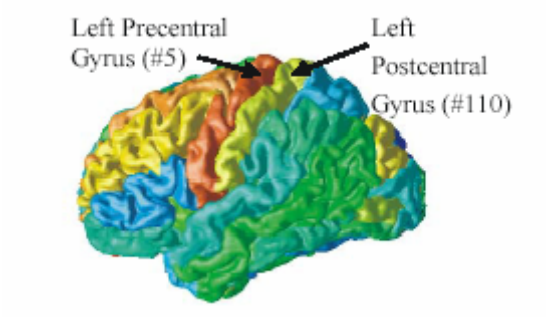

Fig 1.5 The precentral and postcentral gyrus.

Radiology:

Radiologically the CS is an important landmark. It separates the frontal from the parietal lobes and is a landmark to consider when localizing brain lesions (Naidich 1991, Naidich and Brightbill 1996).

On MRI the sulcus appears either dark (T1WI, SPGR) or bright (T2WI) due to the presence of CSF on its surface. There are various shapes of the CS. The most common patterns have been described as "omega" shaped, shown in **Fig 1.6** (a), or "lambda" shaped, shown in **Fig 1.6** (b). These shapes are not so common and the pattern may vary so much that it is almost impossible to have any certainty in identifying the CS based purely on these patterns.

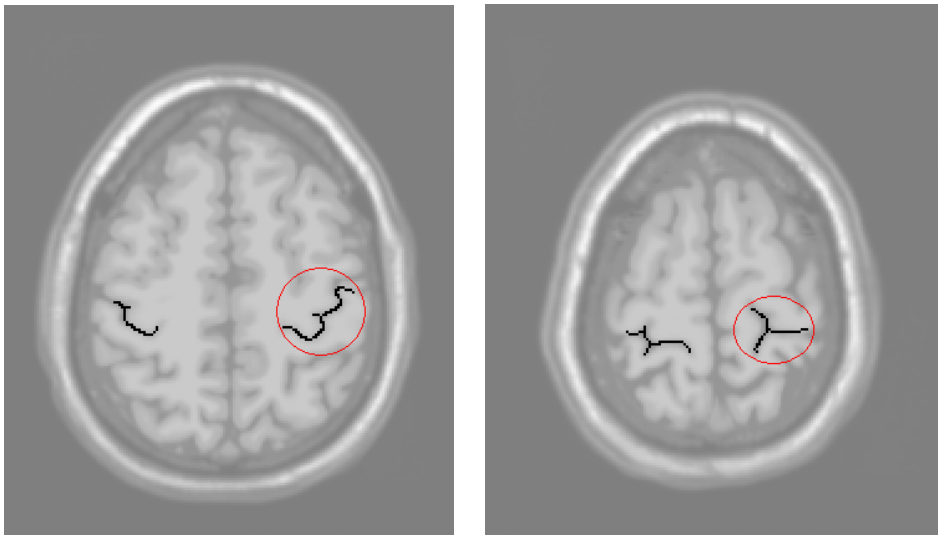

(a) (b)

Fig 1.6 The shapes of the CSs: (a) "omega" shaped CS; (b) "lambda" shaped CS.

The CS is the only sulcus that divides the brain at its superior surface (Naidich and Brightbill 1996). Thus, it is the only sulcus that lies in the coronal plane that runs from the lateral part of the brain to the midline. This feature may be exploited in the identification of the CS.

1.2 Motivation

The CS is one of the most important anatomical landmarks of the cerebral cortex. Its significance lies in its proximity to the pre- and post-central gyri, which contain structures responsible for motor and sensory control. Many other anatomical landmarks in the brain are described in relation to the CS, which must be defined first when a functional representation, an anatomical landmark, or a pathological entity needs to be localized anatomically.

The CS is the major sulcus on the medical aspect of the occipital lobe. Its localization is important as it separates the sensory from the motor areas, whose identification is of primary importance in neurosurgery. For example, the identification of the CS is required for safe treatment of brain lesions near the sensorimotor cortex; it is also important for epilepsy surgery to avoid postoperative functional deficits in children with medically intractable extratemporal lobe epilepsy.

Lesions in the frontal lobe are serious since they may cause disturbance of motor function (loss of fine movements and strength, poor voluntary eye gaze and corollary discharge), environmental control of behavior (risk taking and rule breaking), loss of divergent thinking, poor temporal memory and altered sexual behavior.

Segmentation and identification of the CS is, therefore, crucial.

1.3 Objective of Research

The aim of this project is to design and develop an algorithm (system) to segment and identify the CS without any human intervention. This system can reformat the dataset, remove the skull and other non-brain tissues in order to get a mask of the brain tissues, classify the different brain tissues, get the reference slice and 3D boundary look-up table, segment all the sulci in the region of interest (ROI), identify the CS, remove the over-segmentation and skeletonize the CS in order to remove the unnecessary GM. Through this algorithm we are able to study the relation of the location between the majority of the CS and the anterior and posterior commissures (AC, PC); analyze the 3D volume information of the CS compared to the other major sulci; and test the influence of noise and inhomogeneity.

Some phantom and actual 3D brain MRI datasets have been tested and results are rendered both in 2D slices and 3D model.

1.4 Thesis Outline

In this dissertation, Chapter One briefly presents an overview of the subject of the research under investigation. It also includes the motivation to carry out the investigation and the goals of the research.

Chapter Two introduces the domain knowledge about the anatomy and radiology of the CS, and the MRI techniques are briefly described. It also reviews the trends and recent development of the methods and the history of the identification of the CS in

different medical imaging techniques.

Chapter Three describes the methods of our research and related techniques. The problems of this project are introduced first. Then, the main idea of the algorithm for the whole system and the anatomic knowledge which is useful in our approach is summarized. Third, the detailed method, including tissues classification, region growing, and morphological extraction is presented.

Chapter Four focuses on the pre-processing for the whole approach done in 3 steps: data reformatting, removing the skull and getting the 3D mask of the brain tissues with the help of histogram and morphological processing.

Chapter Five describes the key processes of our approach, including the definition of the desirable ROI, 3D region growing with both CSF and GM, calculation and comparison of the 3D volume of the sulci, setting reference axial slice and 3D boundary look-up table, skeletonization using Hilditch's method and the algorithm to remove the over-segmentation due to the leakage.

Chapter Six presents the results of the experiments, discussion, conclusion and future study.

Chapter 2

Literature Review

2.1 Identification of the CS from Medical Images

The CS can be identified by examining axial slices. Looking at a normalized brain (Talairach and Tournoux 1988), the CS is the easiest to spot on an axial slice with a Z-coordinate (superior –inferior) around 60 mm above the AC-PC plane (Naidich and Brightbill 1996). At this position the superior frontal sulcus can be seen transecting the precentral sulcus (PreCS), and the intraparietal sulcus (IPS) can often be seen to connect with the postcentral sulcus (PoCS). The CS looks more crooked than the flanking PreCS and PoCS - it often contains an *'inverted omega'* shape - which is the landmark for the precentral gyrus's motor-hand area. The precentral gyrus is usually larger than the postcentral gyrus. Furthermore, at this slice, the central sulcus is usually deeper and more continuous than either the PreCS or PoCS. Identifying the PreCS, CS and PoCS is useful, as these areas indicate the location of the primary motor cortex. The precentral gyrus (the gyrus between PreCS and CS) is involved with motor control (e.g. reaching) and the postcentral gyrus (between CS and PoCS) is involved with sensation (e.g. touch). For example, stimulating the motor hand area with a transcranial magnetic stimulation (TMS) wand will cause the hand to flinch.

There are certain anatomical features that describe the CS. Some of them are summarized here:

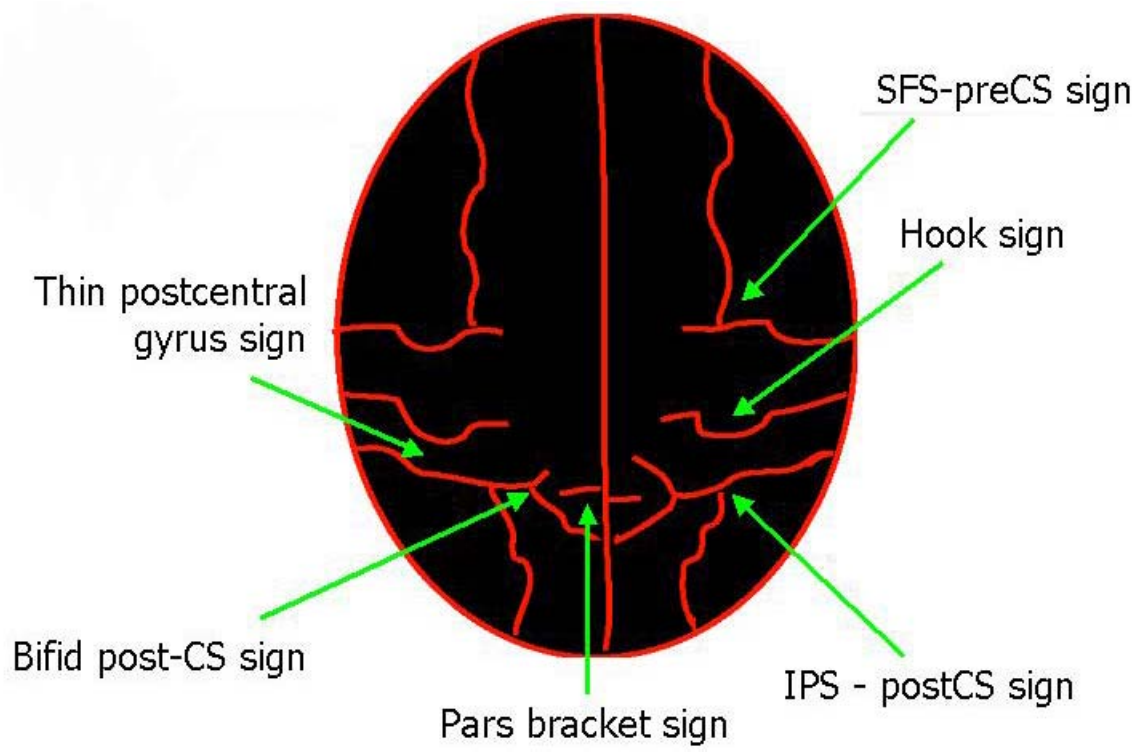

Fig 2.1 Some anatomical features.

1. Superior frontal sulcus (PreCS sign): The posterior end of the superior frontal sulcus joins the precentral sulcus in 85%, shown in **Fig 2.1**.

2. Sigmoid "Hook": Hook like configuration of the posterior surface of the precentral gyrus. The "hook" corresponds to the motor hand area and is well seen on CT (89%) and MRI (98%), shown in **Fig 2.1**.

3. Pars bracket sign: The paired pars marginalis form a "bracket" to each side of the interhemispheric fissure at or behind the CS (96%), shown in **Fig 2.1**.

4. Bifid post-CS sign: The post-CS is bifid (85%). The bifid post-CS encloses the lateral end of the pars marginalis (88%), shown in **Fig 2.1**.

5. Thin post-CG sign: The postcentral gyrus is thinner than the precentral gyrus (98%), shown in **Fig 2.1**.

6. Intraparietal sulcus (IPS) and the post-CS: In axial MRI, the IPS intersects the post-CS (99%), shown in **Fig 2.1**.

7. Midline sulcus sign: The most prominent convexity sulcus that reaches the midline interhemispheric fissure is the CS (70%), shown is **Fig 2.2**:

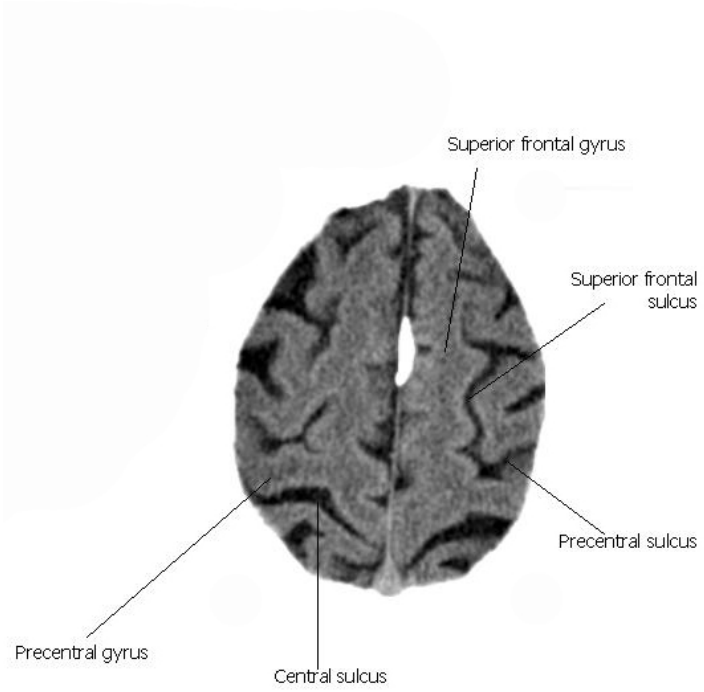

Fig 2.2 Midline sulcus sign.

2.1.1 The Surface Arrangement / Landmarks of the Sulci

Some studies were based on the surface arrangement or landmarks of the sulci.

A lateral axial method is proposed in which the superior frontal sulcus is identified first (Kido et al 1980; Sobel et al 1993). This sulcus forms a right angle with the

precentral sulcus, which is identified next. The sulcus just behind the precentral sulcus is the CS. On images where the CS is difficult to identify because of the difficulty in visualizing the right angle formed by the superior frontal sulcus and precentral sulcus, the right angle formed by the superior frontal gyrus and the precentral gyrus is used as described by Iwasaki et al 1991, on the basis of the pattern of the medullary branches of cerebral white matter.

Another medial axial method, the marginal ramus of the cingulate sulcus is identified first. The sulcus located anterior to it is the CS (Sobel et al 1993).

However, the methods using the surface arrangement or anatomical landmarks are not reliable in cases of brain tumors that compress the CS or other space-occupying lesions. In addition, the variability of sulci and gyri can complicate the identification of the CS considerably.

2.1.2 Pattern Recognition and Statistical Model

Recently, pattern recognition and other techniques have also been applied in this field. Behnke et al 2003 proposed a nearest-neighbor approach, in which a sulcal region is classified as being in the same class as the sulcus from a set of training data which has the nearest pattern of anatomical features (e.g. supramarginal gyrus, cuneus, etc.).

Tao, et al 2001, 2002 built statistical models to extract the sulci. Statistical information of local properties of the sulci, such as curvature and depth, are embedded in these models.

Intraoperative direct cortical mapping is also considered to be a method for

identification of the motor cortex (Berger et al 1997).

2.1.3 Other Medical Modalities

Some other researchers focus on studying the CS by magnetoencephalography (MEG), functional magnetic resonance imaging (fMRI) or somatosensory evoked fields (SEFs).

Chitoku et al. 2000 identify the CS by MEG. In their method, the CS was estimated anterior to the gyrus located somatosensory evoked magnetic field (SEMF) on the surface rendering patient's MR image. Inoue et al. 1999 defined the CS as the nearest sulcus to the N20m for the median nerve stimulus.

Some researchers used fMRI to identify the CS (Cosgrove et al. 1996; Shimizu et al. 1997; Pujol et al. 1998; Inoue et al 1999). In Inoue's approach, the CS is defined as the nearest sulcus to the highest activation spots that were determined by elevating correlation coefficient threshold. Yousry et al. 1996 utilized the central sulcal vein as a landmark for identification of the CS.

The localization accuracy for the CS using the SEFs due to median nerve stimulus has been reported to be highly accurate (Roberts et al. 1995; Kawamura et al. 1996).

In Inoue et al's approach in 1999, the results from the fMRI were accurate in locating the CS in normal cases. However, in some patients' cases, fMRI was not reliable due to venous flow changes by tumor compression and/or compensational activity by brain tissues surrounding the primary sensorimotor cortex.

2.2 Segmentation of the Sulcus/Sulci from MR Images

There are some work on automatic segmentation of sulci on segmentation of the CS. Lohmann and Cramon (2000) proposed to segment the sulcal basins which were the union of all the sulci and GM. Rettmann et al. (2002) used watersheds to segment the sulcal regions which were essentially the union of sulci and GM as well. Mangin et al. (1995) used k-means to find the union of sulci and GM. Renault et al. (2000) proposed curve tracking for sulci detection. Lohmann (1998) proposed to extract sulcal lines. All these methods could not find any specific sulcus and the CS due to the partial volume effect of the MR images.

Manceaux-Demiau et al. (1998) proposed to quantify the CS through probabilistic geometric features like curvature through training provided that the segmentation is available.

There is no method identifying and localizing the CS from MR images automatically.

2.3 Summary

There have been many approaches published to segment the sulcus and identify the CS, since the CS is one of the most important anatomical landmarks of the cerebral cortex.

However, the current approaches suffer from the following limitations:

- Automation problem. The identification of the CS in previous work was either manually by experts, or by other imaging modalities (fMRI, MEG, SEF, brain

mapping etc.). The automatic identification of the CS hasn't been achieved in MRI before.

- Lack of attention on the 3D information of the sulci. The previous analysis of the sulci was mainly focused on 2D features, for example length or area, while the 3D features, such as 3D volume was often ignored.
- Noise and inhomogeneity. The noise and inhomogeneity are inherent features of MRI study and can not be ignored. Many studies have addressed these issues but have not given enough analysis under different noise and inhomogeity levels.

We proposed a new knowledge-driven algorithm to identify and segment the CS automatically from MR images to overcome these limitations.

Chapter 3

Method

3.1 Overview of the Algorithm

Our method is based on the following anatomic facts: (1) the majority of the CS is located between the coronal planes passing AC and PC; (2) the CS has the largest 3D volume among all the sulci in the ROI. These are the basic idea to identify the CS in our approach. Region growing (2D/3D) is the key technique in segmentation of the CS.

The classification of the brain tissues is mainly based on the OTSU (Otsu, 1979) method (which is a thresholding method) and the constrained OTSU method (Hu and Nowinski, 2004). This unsupervised method provides a fast clustering for the voxels in the MR images, and the result can meet the requirement for segmentation.

The main difficulty in segmenting the CS is how to deal with the broken part of the sulci. Due to partial volume effect, noise and inhomogeneity, the sulci are often unconnected in MR images. Our solution is to combine GM into the growing of CSF (sulci) to connect the broken parts, and to apply skeletonization to remove unnecessary GM component. The final CS result includes the skeleton and the CSF component which is connected to the skeleton. Only the necessary component of GM remains to keep the connectivity of the sulci.

The processing steps of our algorithm are diagrammed in **Fig 3.1**.

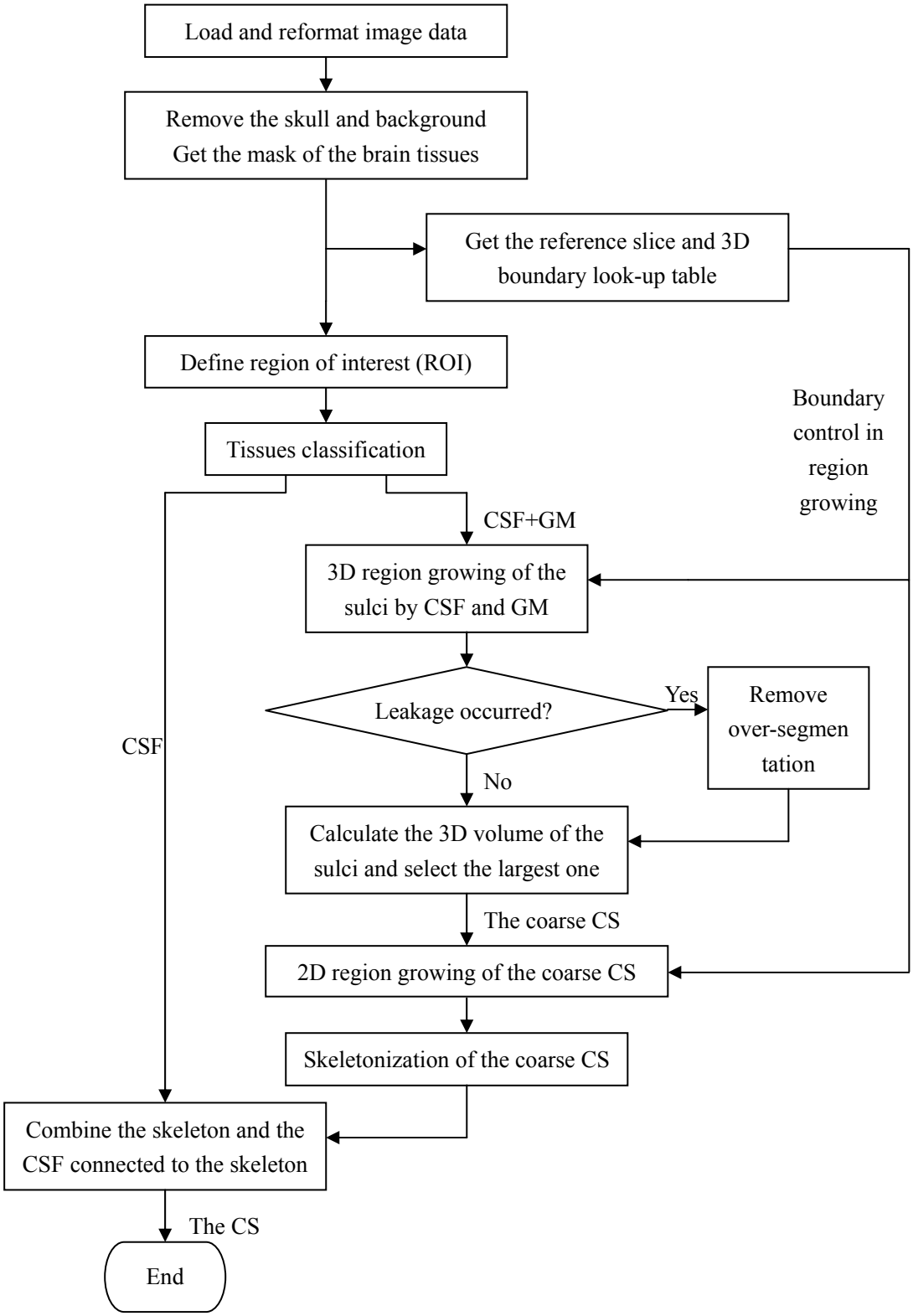

Fig 3.1 The main flowchart of our algorithm**.**

The boundary look-up table, together with an over-segmentation-removal algorithm we designed is applied to constrain the region growing to prevent the over-segmentation. The skull and background voxels are removed and the mask of the brain tissues is obtained through morphological processing.

3.2 Anatomic Knowledge

This is a knowledge-driven approach, so anatomic knowledge of the human brain is an indispensable part of the algorithm. Applying the right knowledge of the human brain features helps to find effective solution and achieve better results.

3.2.1 The Spatial Relationship between the CS and AC-PC

The AC and PC are important landmarks of the brain, shown in **Fig 3.2**.

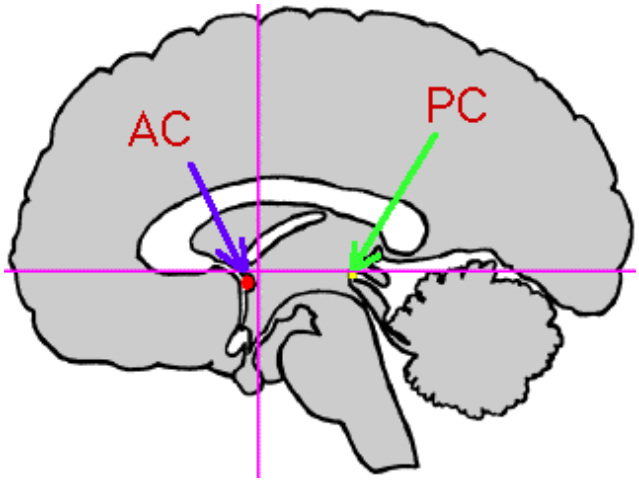

Fig 3.2 The location of the AC and the PC (AC: shown on the left) ; PC: shown on the right).

The location of the CS has a close relationship with the AC and PC. The majority of the CS is between the coronal planes passing through the AC and PC (Talairach and Tournoux 1988). Fig 3.3 shows examples which demonstrate the location of the CS between the coronal planes passing through the AC and PC.

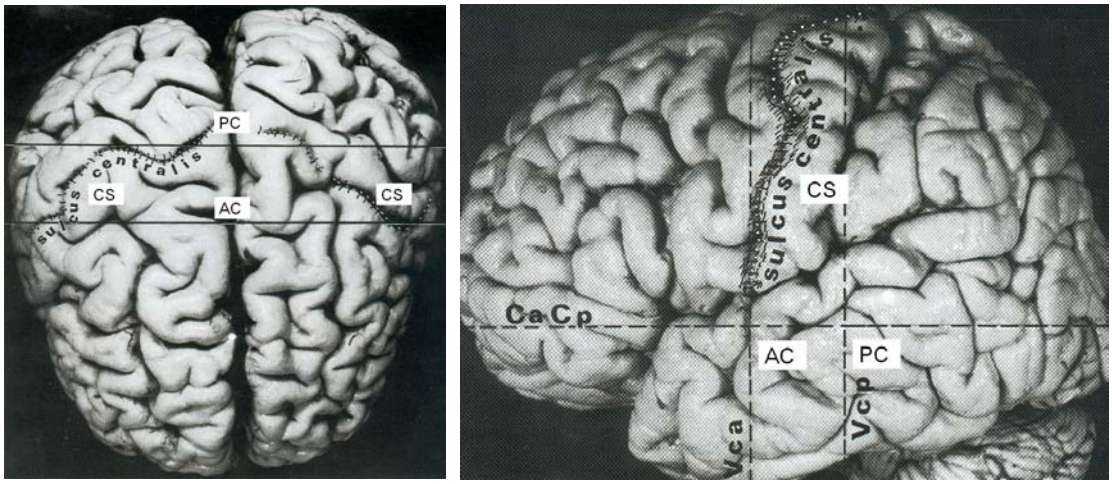

(a) (b)

Fig 3.3 Examples demonstrating the location of the majority of the CS between coronal planes passing through the AC and PC: (a) Top view; (b) Lateral view.

Using the normalized proportional grid system, the statistical location of the CS were obtained for 20 cases of brains stereotactically localized (Talairach and Tournoux 1988) as shown in **Fig 3.4**. That is to say, the majority of the CS is located between the coronal planes passing through the AC and PC in most cases. Thus, the location of the CS can be confined by the coronal planes passing through the AC and PC.

The volume between the coronal planes passing through the AC and PC can be defined as the region of interest (ROI) for subsequent processing. Since the statistical study shows that some part of some CSs will be posterior to the PC, the ROI may be expanded so that some region posterior to the PC will be included.

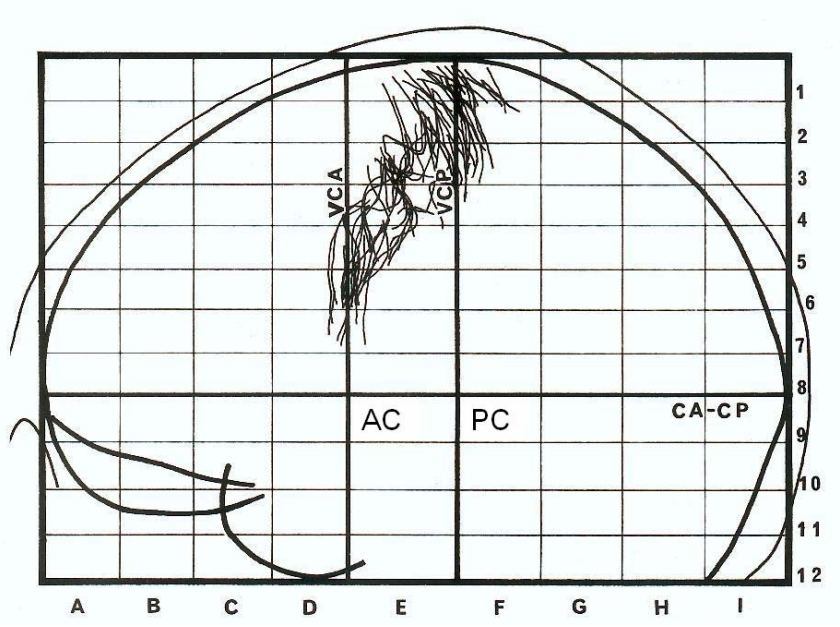

Fig 3.4 The statistical location of the CS for 20 cases.

3.2.2 The 3D Volume of the Sulci

The study of the 3D volume information of the sulci is a contribution of this project. There are 14 major sulci in human brain. Main sulci are formed early in development, and fissures are really deep sulci. In the ROI defined above, the main sulci include the CS, PreCS and PoCS as shown in **Fig 3.5**.

The CS has the largest 3D volume among all the sulci in the ROI defined above, because

1. The CS is a prominent fissure which separates the frontal from the parietal lobes. It is very deep.

2. The CS is a generally continuous sulcus, which increases its volume while the PrCS and PoCS are discontinuous sulci (Ono et al. 1990).

3. The majority of the CS locates within the ROI above, while only a part of the PrCS and PoCS is within this ROI.

Our tests on different data sets has proved that the 3D volume of the CS is the largest among all the sulci in the ROI we defined, which can be an effective method to automatically identify the CS from MR brain images. The detailed testing results of this method will be presented in the next chapter.

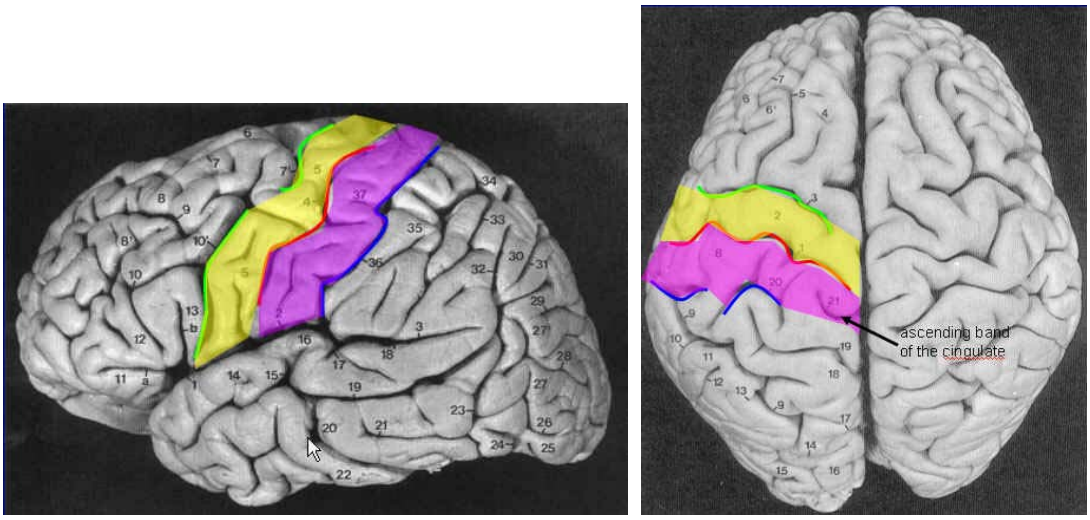

Fig 3.5 Some main sulci: the CS (red), the PoCS (blue) and the PreCS (green)

3.3 Region growing (2D/3D)

Region growing is the key technique in segmentation of the CS in our approach. This is a procedure that groups pixels or sub-regions into larger regions. The simplest region growing starts with a set of "seed" points and from these grows regions by appending to each seed point those neighboring pixels that have similar properties (gray level in our approach).

In our implementation, we designed an algorithm using the linked list class (in Java) to realize the region growing process as the following:

create an empty linked list;

add the seed point (pixel or voxel) into the linked list;

while (the linked list is not empty)

{

remove and return the first element of the list, denoted as ThisPoint;

try {

label ThisPoint as segmented;

for (every neighbor point of ThisPoint, denoted as NP)

{

if ((NP is unlabeled)&&(NP meet the criteria required, gray level etc.))

append NP to the end of this list;

}

catch (exception)

}

Since there is only 2D point class defined in Java, we construct a 3D point class (denoted as Point3D) in order to process 3D region growing:

```
class Point3D {
        public int xx;
        public int yy;
        public int zz;
        public Point3D() {
        }

        public Point3D(int x0,int y0,int z0) {
            xx = x0;
            yy = y0;
            zz = z0;
        }
    }
```

3.4 OTSU Method

3.4.1 Traditional OTSU

OTSU is a nonparametric and unsupervised method of automatic threshold selection (Otsu, 1979). Optimal threshold(s) are to be selected by the discriminant criterion so as to maximize the separability of the resultant classes in gray levels.

Assume that the pixels are represented in L gray levels [1, 2, …, L]. The number of pixels at level i is denoted by n_i and the total number of pixels by $N = n_1 + n_2 + ... + n_L$. The gray-level histogram is normalized and regarded as a probability distribution:

$$p_i = n_i / N, \qquad p_i \geq 0, \quad \sum_{i=1}^{L} p_i = 1. \tag{3.1}$$

Assume that thresholds k_1, k_2 classify the pixels into 3 classes: C_1, C_2 and C_3, then the probabilities of class occurrence and the class mean levels are given by:

$$\omega_1 = \Pr(C_1) = \sum_{i=1}^{k_1} p_i \ , \quad \omega_2 = \Pr(C_2) = \sum_{i=k_1+1}^{k_2} p_i \ , \quad \omega_3 = \Pr(C_3) = \sum_{i=k_2+1}^{L} p_i \tag{3.2}$$

and

$$\mu_1 = \sum_{i=1}^{k_1} i \Pr(i|C_1) = \sum_{i=1}^{k_1} iP_i / \omega_1$$

$$\mu_2 = \sum_{i=k_1+1}^{k_2} i \Pr(i|C_2) = \sum_{i=k_1+1}^{k_2} iP_i / \omega_2$$

$$\mu_3 = \sum_{i=k_2+1}^{L} i \Pr(i|C_3) = \sum_{i=k_2+1}^{L} iP_i / \omega_3 \tag{3.3}$$

And the total mean level of the original picture is as the following:

$$\mu_T = \mu(L) = \sum_{i=1}^{L} iP_i \tag{3.4}$$

The between-class variance of levels is defined as

$$\sigma_B^2 = \omega_1(\mu_1 - \mu_T)^2 + \omega_2(\mu_2 - \mu_T)^2 + \omega_3(\mu_3 - \mu_T)^2 \quad (3.5)$$

Then， the optimal thresholds k_1, k_2 are chosen such that the variance is maximized

$$\sigma_B^2(k_1^*, k_2^*) = \max_{1 \le k_1 < k_2 \le L} \sigma_B^2(k_1, k_2) \quad (3.6)$$

3.4.2 Constrained OTSU

In some subsequent processes of the our approach, the constrained OTSU (Hu and Nowinski, 2004) is applied in order to get more accurate threshold for CSF.

The constrained OTSU is a knowledge-based method. In certain region, the proportion of the each component can be approximated. Thus, in a estimated range of gray levels (for example, from 1% to 20%), applying the standard OTSU method can get more accurate threshold between 2 classes (for example above, CSF and GM) in order to get a more desirable segmentation result.

3.5 Morphology

3.5.1 Dilation and Erosion

Dilation of the set *A* by set *B*, denoted by $A \oplus B$, is defined as

$$A \oplus B = \left\{ x : (\hat{B})_x \cap A \neq \varnothing \right\} = \bigcup_{a \in B} A_a \quad (3.7)$$

Where *A* and *B* are sets in Z. This definition is also known as ‘Minkowski Addition’.

This equation simply means that *B* is moved over *A* and the intersection of *B* reflected and translated with *A* is found. Usually *A* will be the signal or image being operated on and *B* will be the structuring element (SE). Equation 1 is used to process binary sets of data.

$\hat{B}$ denotes the reflection of B i.e., $\hat{B} = \{x | x = -b, \text{for } b \in B\}$ and $(B)_x$ denotes the translation of *B* by $x = (x_1, x_2)$ i.e., $(B)_x = \{c | c = b + x, \text{ for } b \in B\}$ .. Thus, dilation of *A* by *B* expands the boundary of *A*.

The opposite of dilation is known as erosion. This is defined as:

$$A \ominus B = \{x : (B)_x \subseteq A\} = \bigcap_{x \in B} A_x \tag{3.8}$$

This definition is also known as 'Minkowski Subtraction'. The equation simply says, erosion of A by B is the set of points x such that B translated by x is contained in A. However (2) essentially says that for the output to be a one, all of the inputs must be the same as the structuring element. Thus, erosion will remove runs of ones that are shorter than the SE.

3.5.2 Opening and Closing

Opening generally smooths the contour of an image, breaks narrow isthmuses, and eliminates thin protrusions. Closing also tends to smooth sections of contours but, as opposed to opening, it generally fuses narrow breaks and long thin gulfs, eliminates small holes, and fill gaps in the contour.

The opening of set A by structuring element B, denote $A \circ B$, is defined as

$$A \circ B = (A \ominus B) \oplus \hat{B} \tag{3.9}$$

The closing of set A by struturing element B, denoted $A \bullet B$, is defined as

$$A \bullet B = (A \oplus B) \ominus \hat{B} \tag{3.10}$$

The erosion operation will be applied to expand the CSF component (which is the dark component), so that the CS can be found and extracted more easily.

The opening and the closing are the powerful tools in removing the skull, getting the mask of the brain tissues and getting the boundary look-up table.

Chapter 4

Removal of the Skull and Other Non-Brain Tissues

4.1 Introduction

The disconnection of brain from skull and other head tissues is always a tough process, especially in real MRI data sets. The process is based on the assumption that the brain tissue is the largest connected component in the head image volume.

The pre-processing of the MRI data sets includes 3 steps: data reformatting, removing the skull, and getting the mask of the brain tissues.

4.2 Data Reformatting

The reasons and advantages for data reformatting include:

- To standardize the volume data set (1 mm × 1 mm × 1 mm) in order to simplify subsequent calculation and processing
- To make the midsagittal plane (MSP) parallel to the Y-Z plane (shown in **Fig 4.1**) in the new coordinates system. Thus, finding left or right neighbor points will only need to change the X coordinates (shown in **Fig 4.1**) of the points. The effect of the reformation on MSP is shown in **Fig 4.1**.

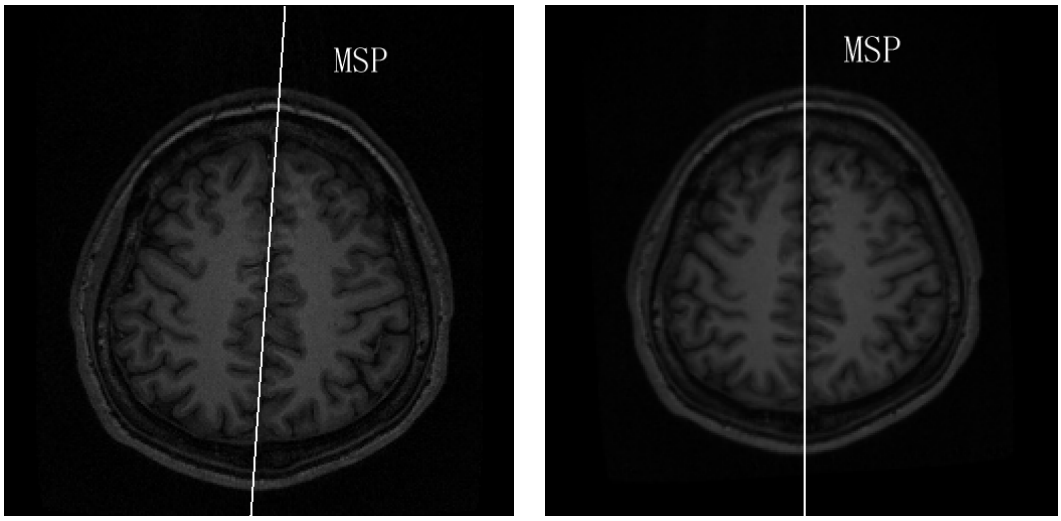

(a) (b)

Fig 4.1 The difference of the MSP due to data reformatting: the MSP in the original data (a) and in the reformatted data (b).

- To make AC and PC in the same horizontal axial slice so that the CS can be easily located, otherwise, the AC-PC line is not perpendicular to the Z direction in the new coordinates system. The ROI between the coronal planes passing through the AC and PC can be described by only Y coordinates of the vertical planes (parallel to the X-Z plane). Fig 4.2 shows the AC-PC line in the same horizontal axial slice after data reformatting and the ROI defined by the Y coordinates of the AC and PC

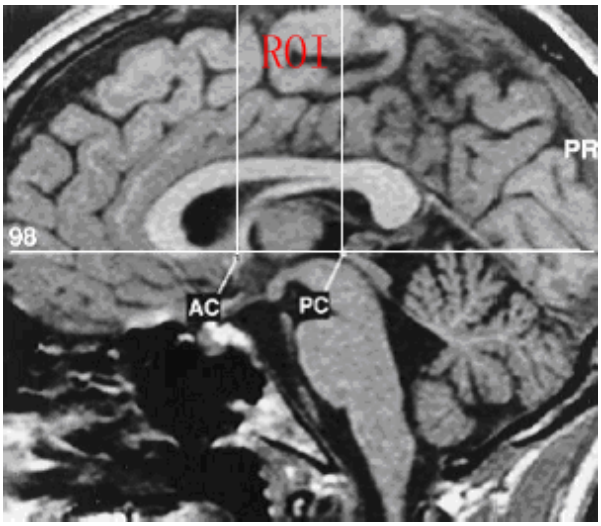

Fig 4.2 The AC-PC line in the same horizontal axial slice after data reformatting and the ROI defined by the Z coordinates of the AC and PC.

After loading a 3D MR volumetric images, the location of the MSP (Hu and Nowinski, 2003), and the coordinates of the AC and PC (Nowinski and Thirunavuukarasuu, 2000) can be determined by our previously developed methods.

1. To normalize the data. Recalculate the new voxels' number (with the size of 1 mm$\times$1 mm$\times$1 mm) in each dimension, according to the actual length of the each dimension respectively. Then, the gray level of each new voxel is determined by the 3D linear interpolation of the gray levels of its 8 neighbor voxels in the original data set. As **Fig 4.3** shown, Assume that B1 is the gray level of an interpolated voxel in the new coordinate system and A1, A2, …, A8 are the gray levels of its neighbor voxels in the original coordinate system. LX, LY and LZ represent the 3D size of the original voxel in x, y, z dimension respectively. Then, B1 could be determined as:

$$B1 = [(LX - x)(LY - y)(LZ - z) \bullet A1 + x \bullet (LY - y)(LZ - z) \bullet A2$$

$$+x \bullet y \bullet (LZ - z) \bullet A3 + (LX - x) \bullet y \bullet (LZ - z) \bullet A4$$

$$+(LX - x)(LY - y) \bullet z \bullet A5 + x \bullet (LY - y) \bullet z \bullet A6$$

$$+x \bullet y \bullet z \bullet A7 + (LX - x) \bullet y \bullet z \bullet A8\,] \;/\; (LX \bullet LY \bullet LZ) \qquad (4.1)$$

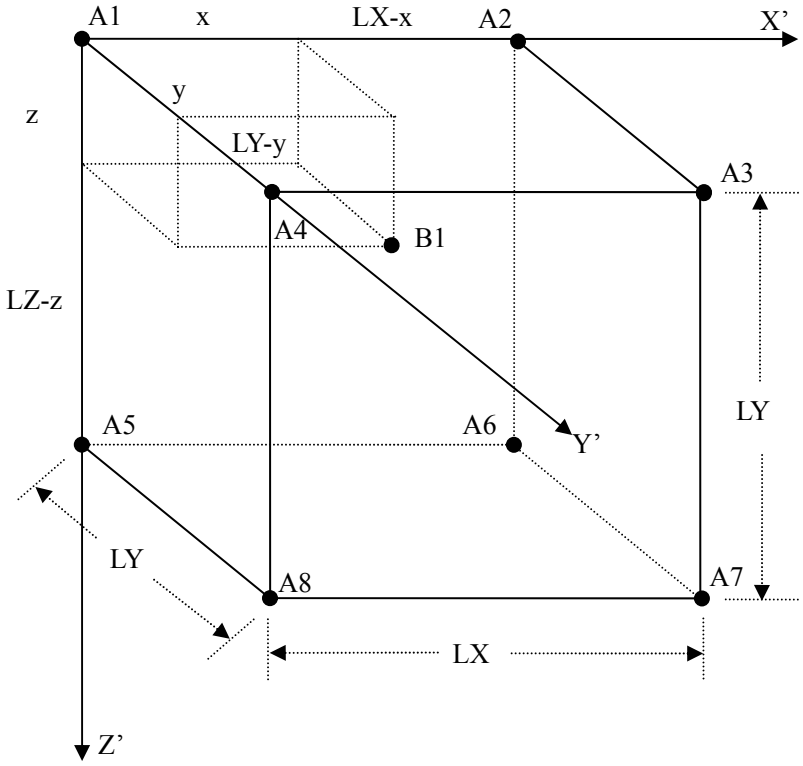

Fig 4.3 The linear interpolation in 3D.

2. Construct the direction vectors for the new coordinate system according to the coordinates of AC-PC and the equation of the MSP, and get the transformation matrix. In the new coordinate system: the X axis has the same direction as that of the normal vector of the MSP; Y axis has the same direction as that of the line connecting the AC and PC; and Z axis has the same direction as the cross product of the new X and Y axes, shown in **Fig 4.4**:

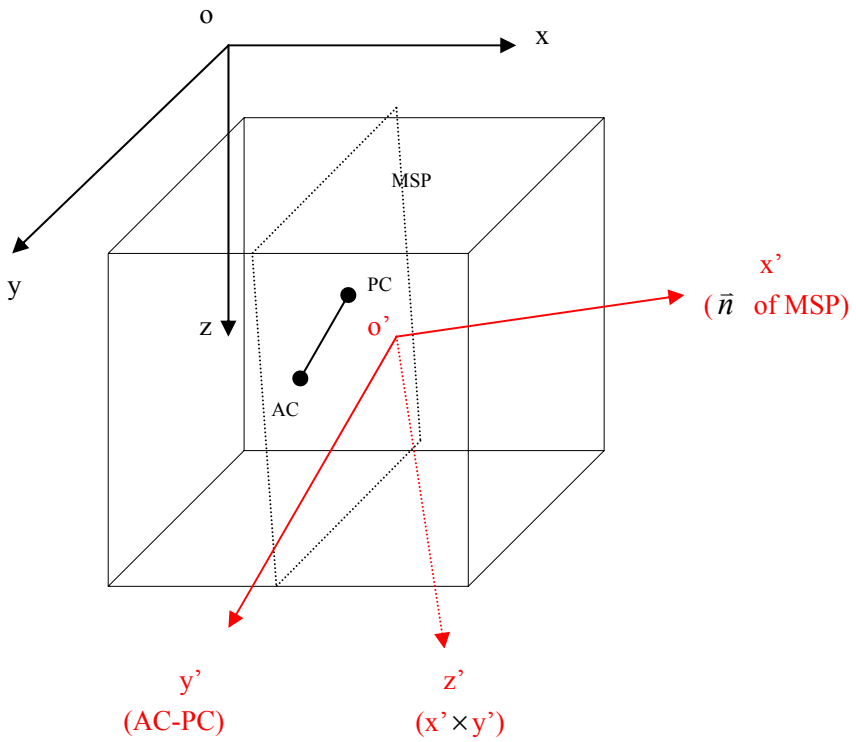

Fig 4.4 The original and new coordinate system of the data set.

Then, the transformation matrix is formed by these 3 directions to transform the coordinates of each voxel in the new coordinate system.

Assume that the MSP equation is as following:

$Ax + By + Cz + D = 0$ (parameter A, B, C and D are normalized with $A^2 + B^2 + C^2 = 1$) (4.2)

Assume the unit direction vector of AC-PC line is (X_1, Y_1, Z_1)

Then, the transformation matrix M is as following:

$$M=\begin{bmatrix} A & B & C \\ X_1 & Y_1 & Z_1 \\ B\times Z_1 - C\times Y_1 & C\times X_1 - A\times Z_1 & A\times Y_1 - B\times X_1 \end{bmatrix} \quad (4.3)$$

3. Transform the coordinates of each point into the new coordinate system using the transformation matrix M.

For each voxel P (x_P, y_P, z_P), it can be projected to voxel P' (x'_P, y'_P, z'_P) in the new coordinate system by

$$P'\ (x'_P, y'_P, z'_P) = P\ (x_P, y_P, z_P)M \quad (4.4)$$

4. Calculate the length of each dimension of the new coordinate system. This length is set as the maximum distance among the all the voxels in corresponding dimension.

5. Calculate the gray level for each voxel by 3D interpolation and the inverse matrix of M. Assume the M^{-1} is the inverse matrix of M, then for each point P' in the new coordinate system, its projected location P in the original coordinate system can be got through

$$P\ (x_P, y_P, z_P) = P'\ (x'_P, y'_P, z'_P)\ M^{-1} \quad (4.5)$$

Since x_P, y_P, z_P are always not integers, the gray level of each new voxel must be calculated in the original coordinate system, using the 3D interpolation of its 8 neighbor original points, which is similar to the procedure above.

For those new voxels, whose original locations are beyond the original data size, set their gray levels as 0.

4.3 Removal of the Skull

In our approach, we need to remove the skull and get the mask of the brain tissues.

The OTSU method is applied first to roughly classify all the voxels in the data into three assumed classes: background, CSF and GM, WM and skull (bones). Of course the two thresholds are not exact for pure purpose of tissue classification, but it is accurate enough to remove the skull.

First select a reference axial slice to start. In our work, the axial slice passing AC-PC is selected. The skull has highest gray level in T1-weighted MR images. So starting from the middle of the left or right edge of the image (the reason to start from this location is that the skull here is the thickest and has least possibility to be broken, shown as **Fig 4.5 (a)**), scan along the X direction, until find a seed whose gray level belongs to the range of skull/WM, as well as its neighbor points, in order to counteract the effect of noise. Then, perform a 3D region growing from this seed, with the criterion that all the grown voxels have the gray level within the range of skull/WM. Of course, these grown voxels should be above the AC-PC axial slice, because there is no or little CS component below this axial slice.

Thus, a 3D hemisphere of the skull is got, although there may be some part broken somewhere, which means the skull we got may not be closed, as shown in **Fig 4.5 (a)**. For this frequent situation, we used 2 methods to counteract it:

The first one is the morphologicalal method. Using a large SE, for example $5\times5\times5$ or $7\times7\times7$ or even larger, let it go through all the voxels and take the closing operation. Then, the original skull is expanded and the broken part is closed, shown in **Fig 4.5 (b)**.

Since this closed skull is expanded, an opening operation with the same SE used

above is followed on this expanded skull. Then, the final skull is got, shown as **Fig 4.5 (c)**, which is the closed skull at almost the same size as the original one. Its shape is a hemisphere, from the AC-PC axial plane to the top slice with the tissues.

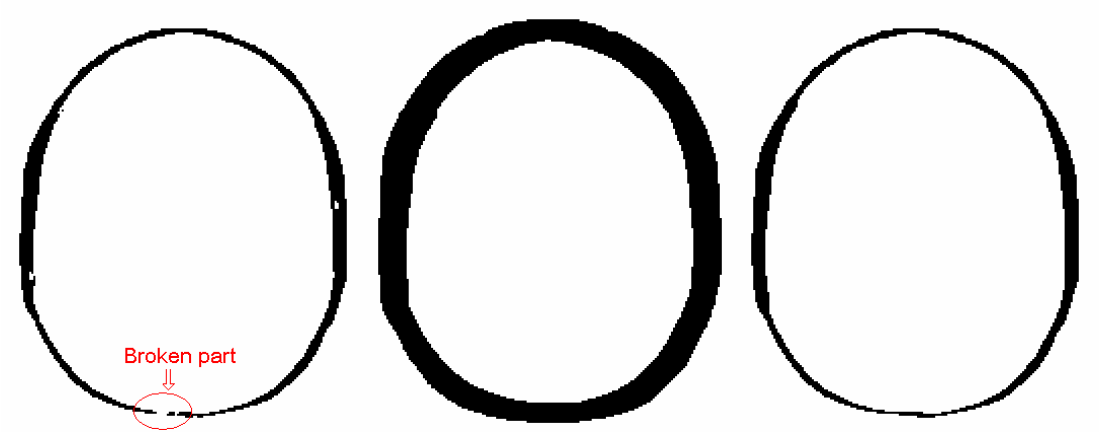

(a) (b) (c)

Fig 4.5 The morphologicalal procedure to close the skull: (a) Original grown skull with broken part; (b) Skull after closing operation; (c) Skull after opening operation.

If the final skull is closed, the skull removal is simpler: we only need to keep the voxels inside the skull and remove the skull and the voxels outside of it (background). But if in case the broken part is large enough and unclosed after morphologicalal processing, another method is designed, followed after the opening operation.

This second method is based on multiple directions tracing.

As shown in **Fig 4.6**, for each voxel inside the skull we extracted (whose shape is like a hemisphere), the skull can be traced in 5 directions: left, right, front, back and up, if the skull is fully closed. But for any non-skull voxel, if the skull can be traced in only 3 out of all these 5 directions, this voxel can still be asserted to be inside of this hemisphere skull. So we just need to trace the skull in 5 directions, if the skull can be

reached in any 3 of them, set this point inside of the skull; otherwise, it is outside. Thus, even though the skull is unclosed in some parts, the non-skull voxels can still be judged if they are inside or outside the skull.

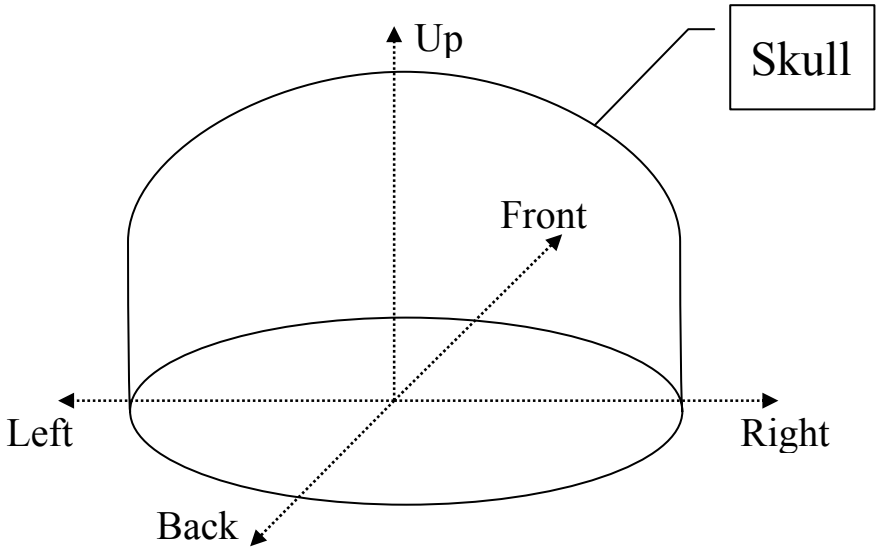

Fig 4.6 The five tracing direction of inside of the skull.

This method has been tested with many data sets successfully.

4.4 Getting the Mask of the Brain Tissues

Getting the mask of the brain tissues is a very important step for our approach. The proper mask can prevent the over-segmentation and calculate the 3D volume of the CS accurately in the following process. Furthermore, the 3D mask of the brain tissues can tell the number of the first top axial slice which contains the brain tissues, which can help a lot in defining the reference slice number mentioned in next chapter. The

proper mask should include the WM and some component of GM and CSF.

Before getting the mask, the OTSU method is applied on the voxels inside the skull, to get the more accurate thresholds for the CSF (including some air between the brain tissues and the skull), GM and WM.

In our previous work, we tried to use the WM and GM to form the tissue structure to get the mask, shown as **Fig 4.7**. But later some problems arose by using this mask. The region growing of the CS (growing CSF component) is aided by growing the GM at the same time in order to counteract the partial volume effect of MRI. If the mask is constructed by both WM and GM, the contour of the final mask will be surrounded by the GM. So in such a mask, the growing of the CS will easily make the leakage occur, in other words over-segmentation, especially at the contour of the mask. The growing of CSF and GM will often include other sulci such as pre-central sulcus or post-central sulcus since their GM components are connected at the contour.

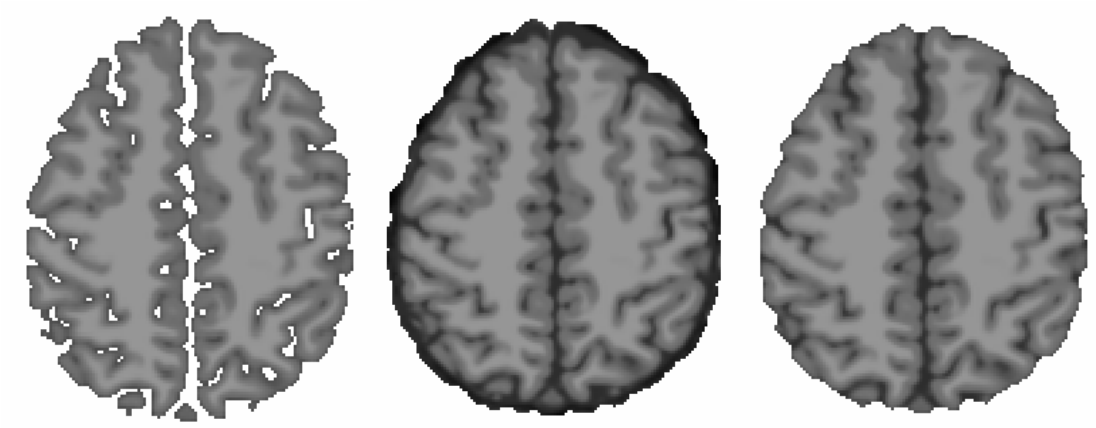

Fig 4.7 Mask construction in previous attempt: (a) WM and GM; (b) The closing result of the structure; (c) The final mask after opening.

So finally only WM is used to get the structure, and the mask is constructed by

applying morphological processing on such a structure. There are two reasons to do so:

1. The brain tissues form the largest connected component in the head image volume and WM is the more reliable structure compared to the other brain tissues.
2. The mask constructed by the WM only will have much less GM on its contour, the CSF and GM components will all be between the gyri formed by the WM. Growing the sulcus in such a mask will not include other sulci, which will prevent the over-segmentation effectively. The calculation of the 3D volume of the CS will be much more accurate by using this mask.

The procedure is as following. For the original MRI data set, shown as **Fig 4.8 (a)**, extract the voxels inside the skull, shown as **Fig 4.8 (b)**. A line parallel to the MSP in an axial slice with a certain distance (5-15 mm) to the MSP will have several intersections with the voxels whose gray levels belong to the WM. In this way seeds of the WM can be found as the intersected voxels. Perform a 3D region growing with the voxels whose gray levels belong to WM from these seeds. Choose the component with the largest 3D volume as the WM, shown as **Fig 4.8 (c)**. 3D spherical SE were constructed. With the help of these structuring elements, we applied 3D closing on the WM followed by opening with the same SE. The final result is the mask of the WM with the sulci (the CS included) and GM, shown as **Fig 4.8 (d)**. The CSF and GM components are all between the gyri of the WM.

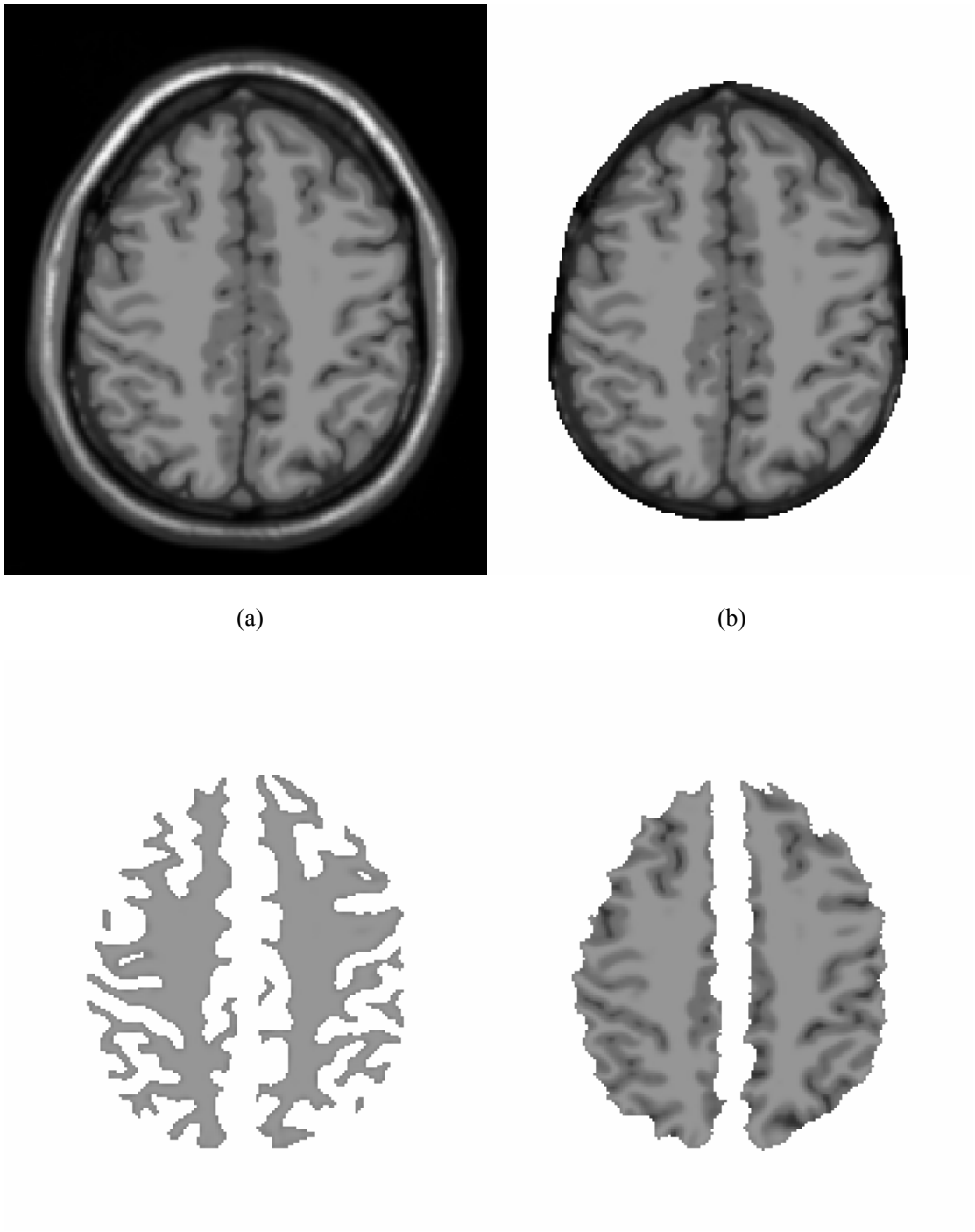

(a) (b)

(c) (d)

Fig 4.8 The procedure to get the mask of the brain tissues by the structure using WM only: (a) Original data; (b) The brain tissues inside the skull extracted from morphologicalal processing; (c) The WM segmented by 3D region growing; (d) The mask of the brain tissues after closing and opening (WM, GM and sulci are included).

After getting the mask, the voxels within this final mask should be classified again. This time all the voxels are almost purely the CSF, GM and WM. Apply the OTSU method again and classify these voxels into three classes.

The thresholds differ from those of the first time. They are more accurate for the CSF, GM and WM. **Fig 4.9** shows the comparison of the results of the two classification procedures in the same phantom dataset. **Fig 4.9 (a)** is the original data set and **Fig 4.9 (b)** is the brain tissues inside the mask. **Fig 4.9 (c)** and **Fig 4.9 (d)** show the histograms of the objects in **Fig 4.9 (a)** and **Fig 4.9 (b),** respectively. The k_1, k_2 are the thresholds. The thresholds in **Fig 4.9 (c)** are accurate enough to remove the background and the skull (classify the skull and the WM as the same class); while the thresholds in **Fig 4.9 (d)** are much more accurate to classify the brain tissues into the WM, GM and CSF, which is very helpful to achieve the exact segmentation result in the subsequent processing.

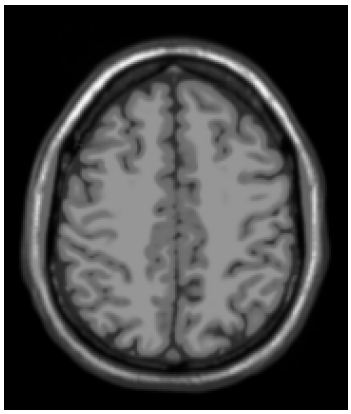

(a)

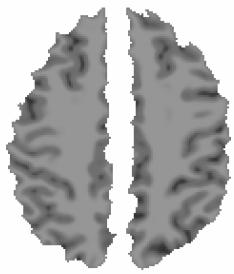

(b)

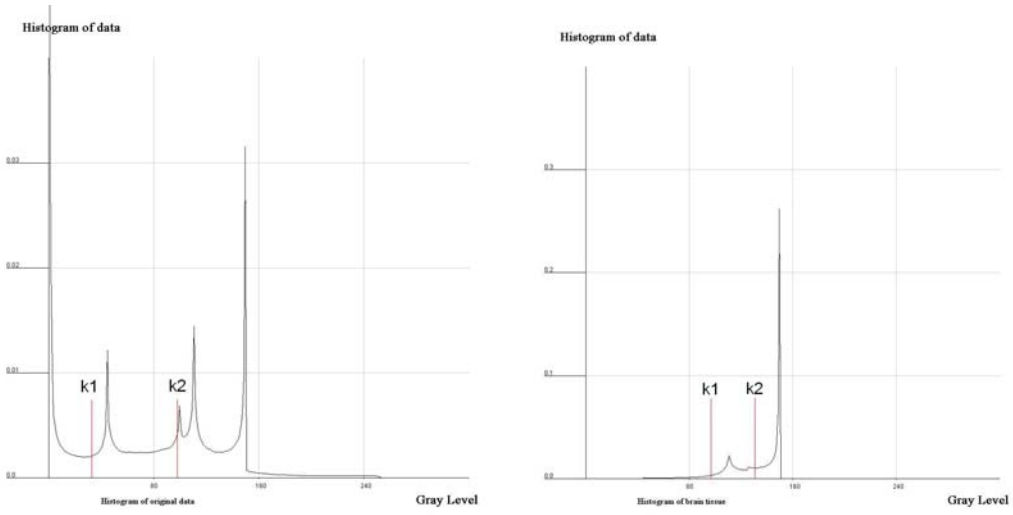

(c) (d)

Fig 4.9 Histogram of the 3D phantom data and the thresholds (k_1, k_2) selected by OTSU method. (a) The original dataset; (b) The brain tissues segmented (inside the mask); (c) The histogram of the original dataset shown in (a); (d) The histogram of the brain tissues shown in (b).

4.5 Summary

Reformatting the data sets is the initial step of the whole approach, which will normalize and adjust the original data in order to facilitate subsequent procedures. After data reformatting, each voxel will have the unit size of 1 mm$\times$1 mm$\times$1 mm, and the AC and PC will be located in the same axial slice.

Removing the skull and getting the mask of the brain tissues is a very important step. The proper mask we get can prevent the over-segmentation and calculate the 3D volume of the CS accurately in the following process. In addition, the 3D mask of the brain tissues can tell the number of the first top axial slice which contains the brain tissues, which can help in defining the reference slice number mentioned in next

chapter. In short, the mask will influence the final segmentation result of the CS.

In our approach, we adjust the standard data reformatting procedure (in which the AC and PC are not located in the same axial slice after reformatting) to facilitate our subsequent processing and improve the process of removing the skull and getting the mask, by applying the morphological processing, multiple directions tracing and recalculating the thresholds.

Chapter 5

Identification and Segmentation of the CS

5.1 Introduction

Since the majority of the CS is between the coronal planes passing through the AC and PC, we define our ROI as the 3D region between these two coronal planes. Our approach is to find all the sulci within this ROI and calculate the 3D volume of each. The sulcus with the largest 3D volume is the CS.

A primary problem in segmentation of the CS is that the partial volume effect may result the broken part of the sulci, which hinders the sulci segmentation using region growing, shown as **Fig 5.1**.

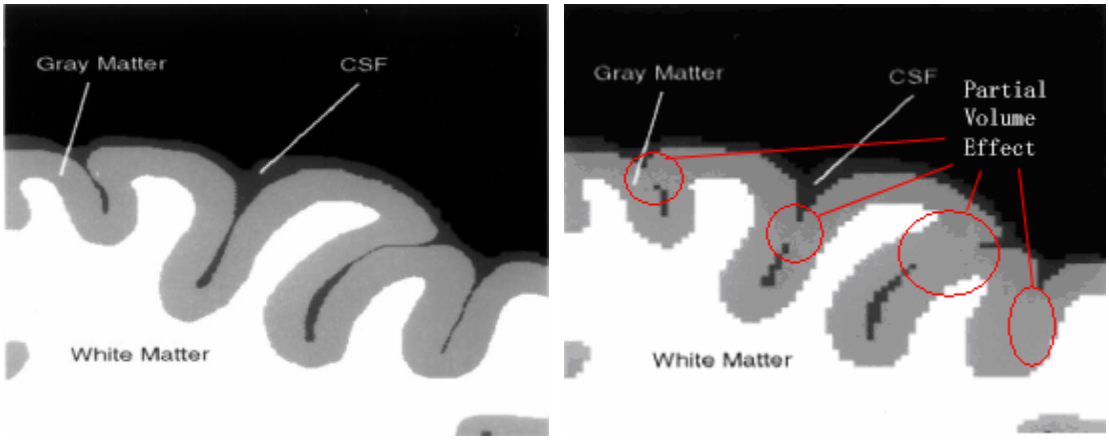

Fig 5.1 The partial volume effect of the MR images: (a) The high-resolution image; (b) The low- resolution image.

Because of the individual variance, sometimes the pre-central gyrus and post-central gyrus is too close, there may be no CSF component in CS. So the CS is a structure

filled with liquid, not a tissue.

5.2 Reference Slice and ROI

In order to find all the sulci in the ROI, a reference slice to initiate the 3D region growing has to be selected. In the desirable reference slice, the CS should be near the MSP and easily traced.

The 3D mask of the brain tissues can tell the top slice containing the brain tissues.

Assume that N_{AC-PC} is the slice number of the axial slice passing through the AC and PC, $N_{TopTissue}$ is the slice number of the top axial slice of brain tissue. Based on the experience of testing a set of images, the number of the axial reference slice could be selected around slice **N**, where

$$\mathbf{N}=\frac{1}{6}*\mathbf{N_{AC\text{-}PC}}+\frac{5}{6}*\mathbf{N_{TopTissue}} \qquad \textbf{(5.1)}$$

In such a reference slice, the CS can be easily traced in the parallel line to the MSP with a distance of 20 mm from it. The experience of selection of the reference slice is got from statistical results based on 20 data sets.

The ROI to segment the CS is the region between the AC-PC coronal planes (in order to include more component of the CS, we usually define y coordinate of ROI between [AC, PC+30mm], which is got from the experience by testing more than 20 data sets), and from the AC-PC axial slice to the top axial slice with brain tissue. **Fig 5.2** shows the ROI we defined (within the black contour) and the location of the CS (indicated in red) in the ROI in several axial slices.

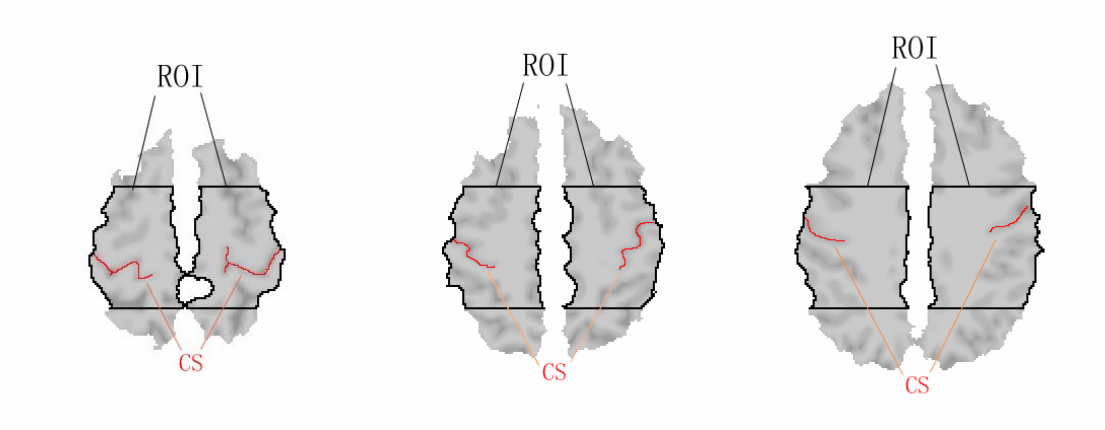

Fig 5.2 The ROI (within the black contour) and the location of the CS (indicated in red) in the ROI in several axial slices.

5.3 3D Look-up Table of the Boundary Voxels

Due to the partial volume effect, sulci may be broken in MR images, so GM is used to aid the segmentation of sulci. To avoid over-segmentation due to GM, we set a 3D look-up table [Hu et al 2001] of the boundary voxels of the brain tissue in order to control the region growing.

A morphological binary opening was applied to the brain tissue mask using a 3D spherical SE with a radius of one voxel ($3\times3\times3$) to find boundary voxels. In other words, for any voxel which is within the 3D mask, only if all its 26 neighbor voxels are all within the 3D mask too, this voxel is not the boundary one. Otherwise, it is labeled as a boundary voxel.

In order to reduce calculation, the 3D look-up table is set as a 3D binary matrix in coding, the elements corresponding to the boundary voxels are labeled as different. Thus, the 3D region growing of the sulci can be within the mask. The boundary voxels can not be grown so that the GM component on the boundary is controlled not

to connected to the other sulci in the same axial slice or sulci in the neighbor axial slice.

5.4 3D Region Growing of the Sulci in ROI

3D region growing was applied to find all the voxels for each sulcus so that its volume can be obtained. The volume of each sulcus is the number of voxels of the sulcus. The CS is the sulcus with the largest volume.

Assume that $x = X_{MSP}$ is the equation of the MSP. In the reference slice we select 2 reference lines $x_1 = X_{MSP} + 20$ and $x_2 = X_{MSP} - 20$, which are the 2 parallel lines to the MSP with a distance of 20 mm to it. Such a distance is obtained from the statistical study of 26 phantom and real datasets. In the reference slice we defined above, the parallel line with such a distance to the MSP will definitely intersect with the CS.

There are several intersected voxels with the reference lines and the sulci within the region between (and near) the AC and PC. Set these intersected voxels as the seeds for the 3D region growing. There is a restricting area that constrains the 3D region growing: the region between $X_{MSP} - 10$ and $X_{MSP} + 10$. So the lines x= $X_{MSP} - 10$ and x= $X_{MSP} + 10$ are the restriction lines. The region growing of the CSs in both hemispheres can not grow in the region between these two lines, otherwise, the space between the two hemispheres is easily connect to the CS in the top slices and the leakage of growing the sulci may occur.

Besides the restriction lines mentioned above, the criteria for region growing also include: (1) the gray level of the voxel must be within the range of the gray level of CSF or GM; (2) the z coordinate of the voxel should not go beyond the range from the z coordinate of the AC-PC to the top axial slice of the brain tissue; (3) the y value of the voxel must be in the range from the y_{AC} to α mm posterior to y_{PC} (y_{AC}, y_{PC} refer to the y coordinates of the AC and PC respectively, α is a statistical parameter which is determined through testing more than 20 data sets, set as 30 in our approach); and (4) the voxel should not go beyond the region defined by the boundary look-up table.

Since the GM is combined with the growing of the CSF, the problems of broken part of the sulci are well resolved. That is because the CSF is always surrounded by the GM and the GM is seldom unconnected. Thus, our method got the completeness of the sulci so that the calculation of the 3D volume can be carried out.

5.5 Removal of Over-segmentation Component

As GM is used in region growing of CSF to counteract the broken sulci due to partial volume effect, over-segmentation may occur when there is noise and/or inhomogenieity. There are two cases of over-segmentation per hemisphere on axial slices: 1) there are more than two segments of the CS (due to 3D region growing), for example shown in **Fig 5.3** (a); and 2) a single segment of the CS exists, but it contains much more component than the CS itself, for example as shown in **Fig 5.3** (b).

A suitable initial slice is assumed as: 1) there is only a single segment of the CS per hemisphere in this slice and its adjacent slices; and 2) the difference in the area (the number of the voxels) of the CS segmented per hemisphere between this slice and each of its adjacent slices will not exceed a certain value β (which is set as β=30% in our approach).

Hence, the processing is as follows. Starting from the initial slice M, set adjacent slice N (N=M-1 or N=M+1). Calculate the number of the segment(s) of the CS per hemisphere in slice N:

Case 1) there is only a single segment of the CS per hemisphere in slice N:

calculate the difference in the area of the CS between slice M and N.

if (the difference is not greater than β)

There is no over-segmentation in slice N.

else if (the difference is greater than β)

dilate the CS in slice M using a SE with a radius of one voxel and process "and" operation between this dilated area and the CS in slice N; take the matching part as the final segmented CS in slice N

Case 2) there are more than one segment of the CS per hemisphere in slice N:

Perform "and" operation between the CS in slice M and N, find and take the segment in slice N which matches the CS in slice M most. Then, process as shown in Case 1 above to get the final CS for slice N.

After detecting and removing the over-segmented component in slice N, set N as the

reference slice and process its adjacent slice(s) in a similar way.

Two examples of over-segmentation are shown on the right hemisphere in **Fig 5.3** (a) (b), and their corrections are presented in **Fig 5.3** (c) (d), respectively.

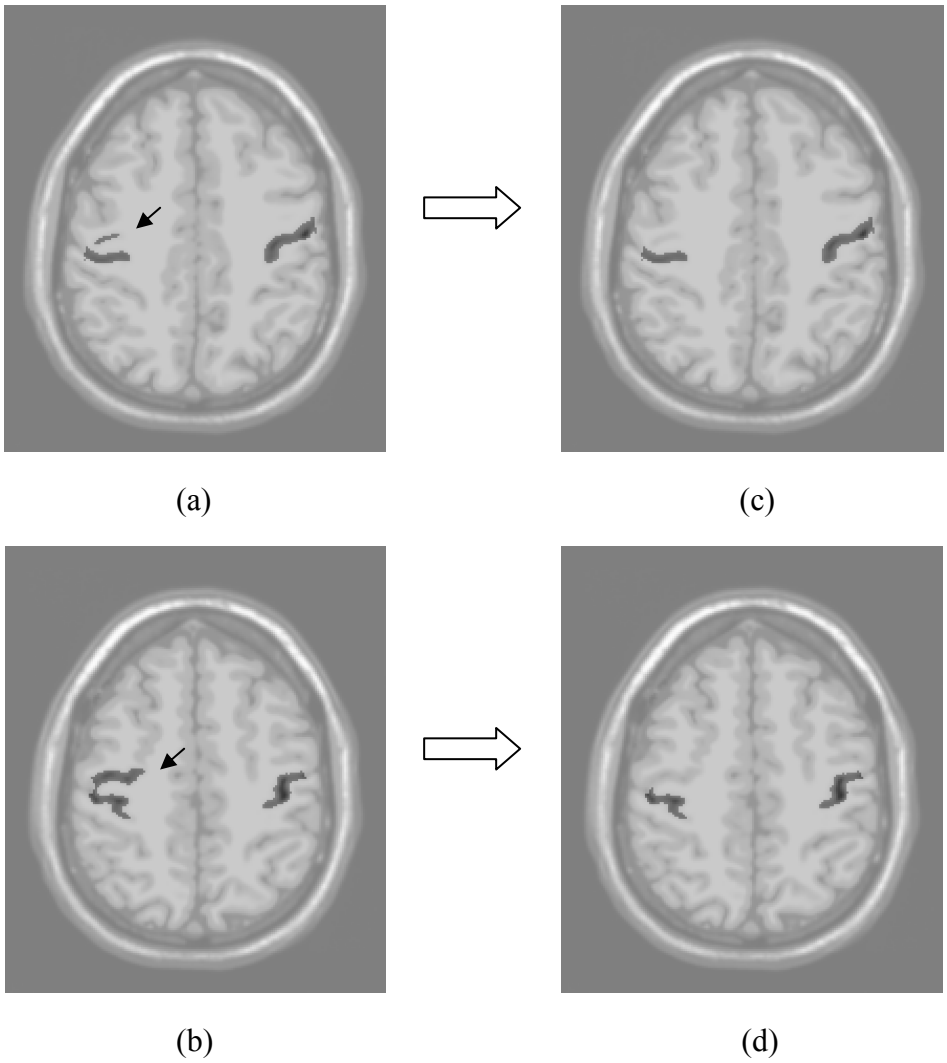

(a) (c)

(b) (d)

Fig 5.3 Removal of over-segmentation: (a) Over-segmentation with multiple segments (indicated by the arrow). (b) Over-segmentation with a single segment (indicated by the arrow). (c) Removal result of over-segmentation of (a). (d) Removal result of over-segmentation of (b).

This method aims to detect and remove the obvious over-segmentation resulted from region growing. It has been tested on more than 20 data sets and proves to be effective.

The limitation of this method is that it can not detect the tiny over-segmentation due to a thresholding problem.

5.6 Identification of the CS

We tried to identify the CS by its geometrical feature: the CS is the most nearest sulcus to the MSP in certain reference axial slices. After quantitative testing on various data sets, we found that the location of those reference axial slices differs a lot among different data sets. For example, the distance from the reference slice to the top tissue slice is about 15 mm among MRI data acquired in Singapore, while this value is about 30 mm among MRI data acquired in Japan.

So now we use a robust feature of the CS to identify it: to compare the 3D volume of the sulci. Among all the sulci within the ROI, the CS has the largest 3D volume. So we just need to calculate the 3D volume (the number of the voxels) of all the sulci in ROI, choose the one with largest 3D volume as the coarse CS and process the following steps.

5.7 2D Region Growing of the Sulci

Although the 3D mask and 3D look-up table of boundary of the brain tissues are helpful in avoiding over-segmentation in 3D, they bring some undesirable effect that excludes some voxels which should belong to the sulci, shown in **Fig 5.4** (a). 2D

region growing in each axial slice is applied after over-segmentation removal to overcome this shortcoming.

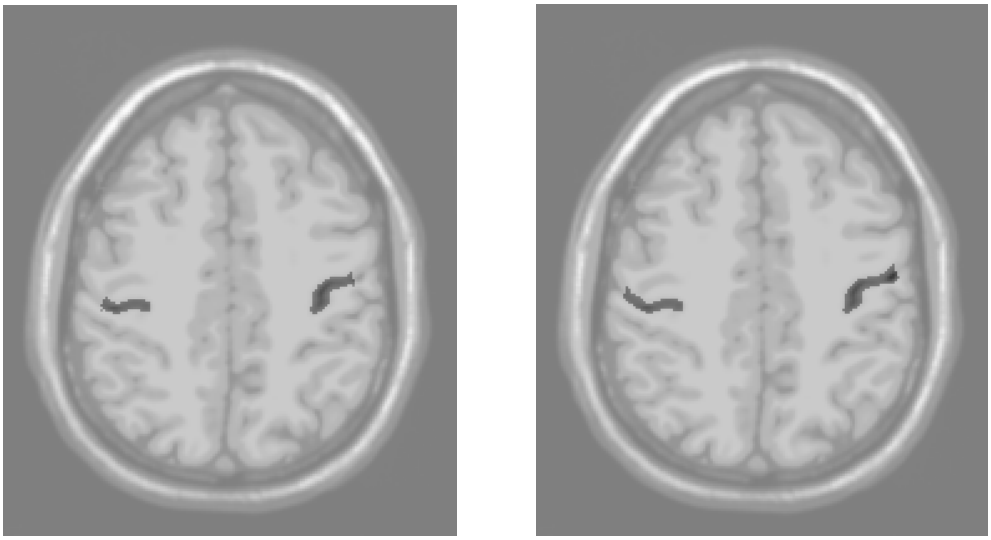

(a) (b)

Fig 5.4 The effect of the 2D region growing: the coarse CSs before (a) and after (b) and 2D region growing.

A dilation using a SE with a radius of one voxel is applied to the original mask. A 2D boundary look-up table can be obtained for each axial slice within the dilated mask in a similar way mentioned before. The sulci component segmented above is used as the seeds, which is grown in 2D with the similar criteria used in previous 3D region growing. After applying the algorithm for over-segmentation removal again, the coarse sulci which including some GM are achieved, shown in **Fig 5.4** (b), which is more exact than those before the 2D region growing which are shown in **Fig 5.4** (a).

5.8 Skeletonization of the Sulci

The GM grown together with the CSF helps to keep the completeness of the sulci, but

among all the GM in the coarse CS, only some should be kept to connect the CS while the other should be removed. Skeletonization is applied, using Hilditch's algorithm (Hilditch 1969), to remove the GM from the coarse CS to get the final CS.

The Hildtch's algorithm is described as follows:

Consider the 3×3 window around a "black" pixel labeled p_1 and label its eight neighbors in a clockwise spiral fashion as illustrated in **Fig 5.5**. Let $A(p_1)$ denote the number of 01 patterns encountered in the $p_2, \ldots, p_9, p_2$. Let $B(p_1)$ denote the number of non-zero neighbors of p_1. Then, at each pass in which we remove (in parallel) the outer layer of pixels we remove each pixel that satisfies the following four conditions:

1) $2 \le B(p_1) \le 6$

2) $A(p_1) = 1$

3) $p_2 \bullet p_4 \bullet p_8 = 0$ or $A(p_2) \ne 1$

4) $p_2 \bullet p_4 \bullet p_6 = 0$ or $A(p_4) \ne 1$

The algorithm stops when there are no pixels changed during a pass.

p_9	p_2	p_3
p_8	p_1	p_4
p_7	p_6	p_5

Fig 5.5 The matrix used in the Hilditch's algorithm.

Explanation of the procedure:

1) The condition $B(p_{1)} \leq 6$ ensures that p_1 is on the boundary of P.

2) The condition $2 \leq B(p_1)$ ensures we keep isolated points as well as skeleton tips.

3) The condition $A(p_1) = 1$ ensures we do not fragment the skeleton.

4) Condition 3) and 4) ensure we do not change the connectivity of "lines" that are two pixels thick.

By applying the skeletonization method, the skeleton of the CS (shown as **Fig 5.6** (c)) is obtained to achieve the final CS result.

5.9 Getting the Final CS

The CSF voxels based on thresholding connected to the skeleton are added to the skeleton to yield the final CS.

Shown as in **Fig 5.6**, **Fig 5.6** (a) is the CSF component based on the thresholding, from which the broken part of the CS can be observed; **Fig 5.6** (b) shows the coarse CS grown by both the CSF and GM, which keep the connectivity of the CS; **Fig 5.6** (c) presents the skeleton of the coarse CS using the Hilditch's method; **Fig 5.6** (d) shows the final CS segmentation result, which combines the skeleton and the CSF component which is connected with the skeleton. Thus, the minimum component is kept in the CS to keep its connectivity and the segmentation result is most desirable.

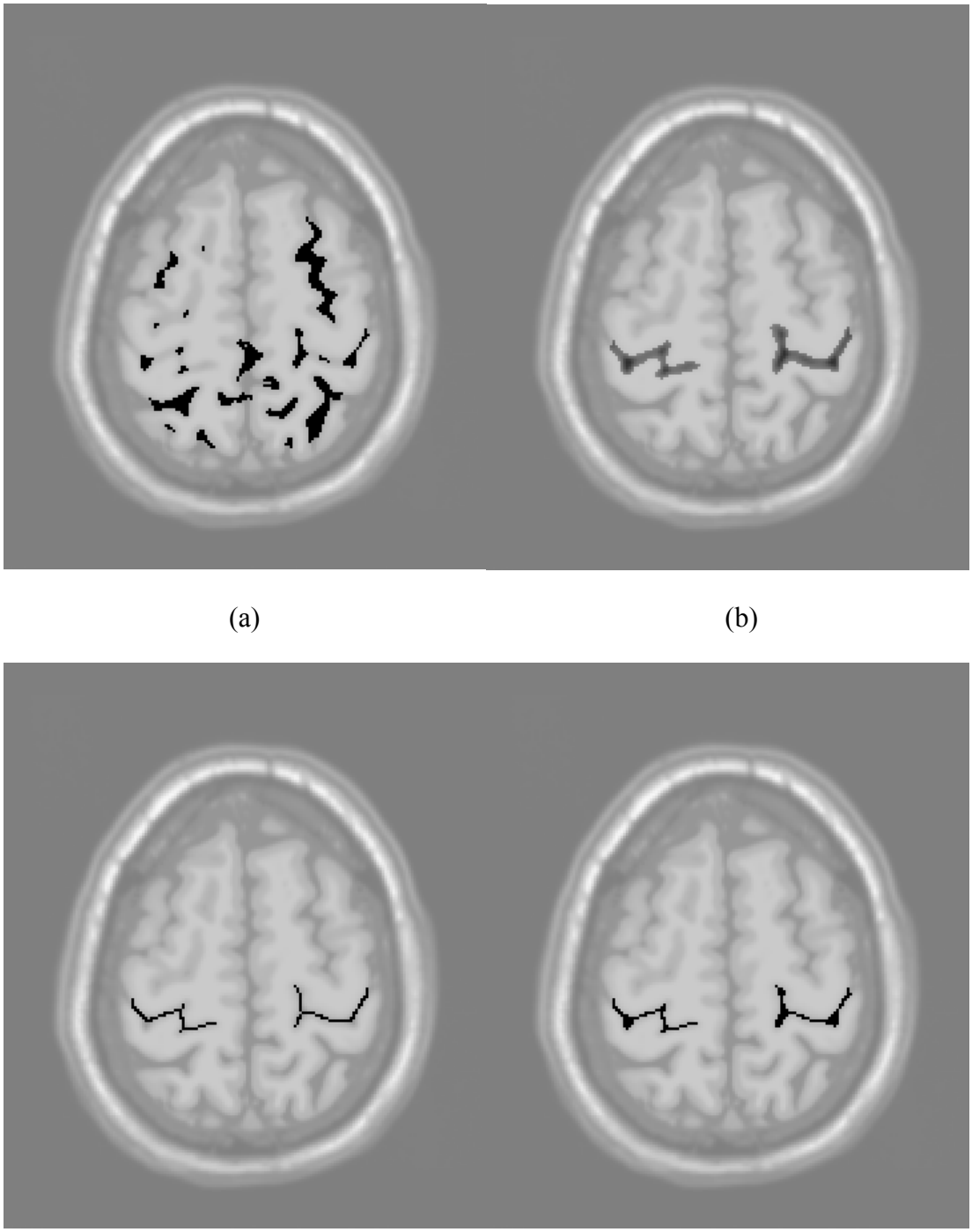

(a) (b)

(c) (d)

Fig 5.6 The final CS: (a) CSF from thresholding. (b) The coarse CS grown by CSF and GM. (c) The skeleton of the coarse CS. (d) The final CS combined by the skeleton and the CSF connected to the skeleton.

5.10 Summary

A primary contribution of our approach is to combine the GM into the region growing of the CSF in order to counteract the broken part of the sulci due to partial volume effect, and the unnecessary GM component is removed through skeletonization while minimum GM is kept to maintain the connectivity of the sulci. So the final segmentation result of the CS is the most desirable while keeping the complete shape of it.

The method to identify the CS by calculating and comparing the 3D volume of the sulci proves to be effective, which is more robust than the other previous methods using the geometrical features of the brain tissue arrangement. Our method can identify and segment the CS automatically and no manual intervention is required.

The algorithm we designed to remove the obvious over-segmentation component also proves to be desirable after quantitative testing. It is especially effective in resolving the over-segmentation problems due to the leakage. Combining our algorithm and the 3D boundary look-up table, the over-segmentation is controlled well to get the accurate calculation and segmentation.

Chapter 6

Results, Conclusion and Prospects

6.1 Results

To evaluate our approach we use a set of T1-weighted phantom data (http://www.bic.mni.mcgill.ca/brainweb/) with noise (0, 1%, 3%, 5%, 7% and 9%) and inhomogeneity (0, 20% and 40%). The advantage of using the phantom data is that its CSF, WM, and GM are known which enables qualitative and quantitative evaluation of our approach. Among the 18 datasets, the CS is successfully identified and segmented from 16 datasets, while failed in 2. Our approach has also been applied on 4 patient-specific datasets.

6.2 Visualization

Fig 6.1 shows the final results of the CS identified and segmented. It shows that the CS is successfully identified and segmented. Compared with manual approaches, the result of our algorithm is visually correct as confirmed by brain anatomy experts.

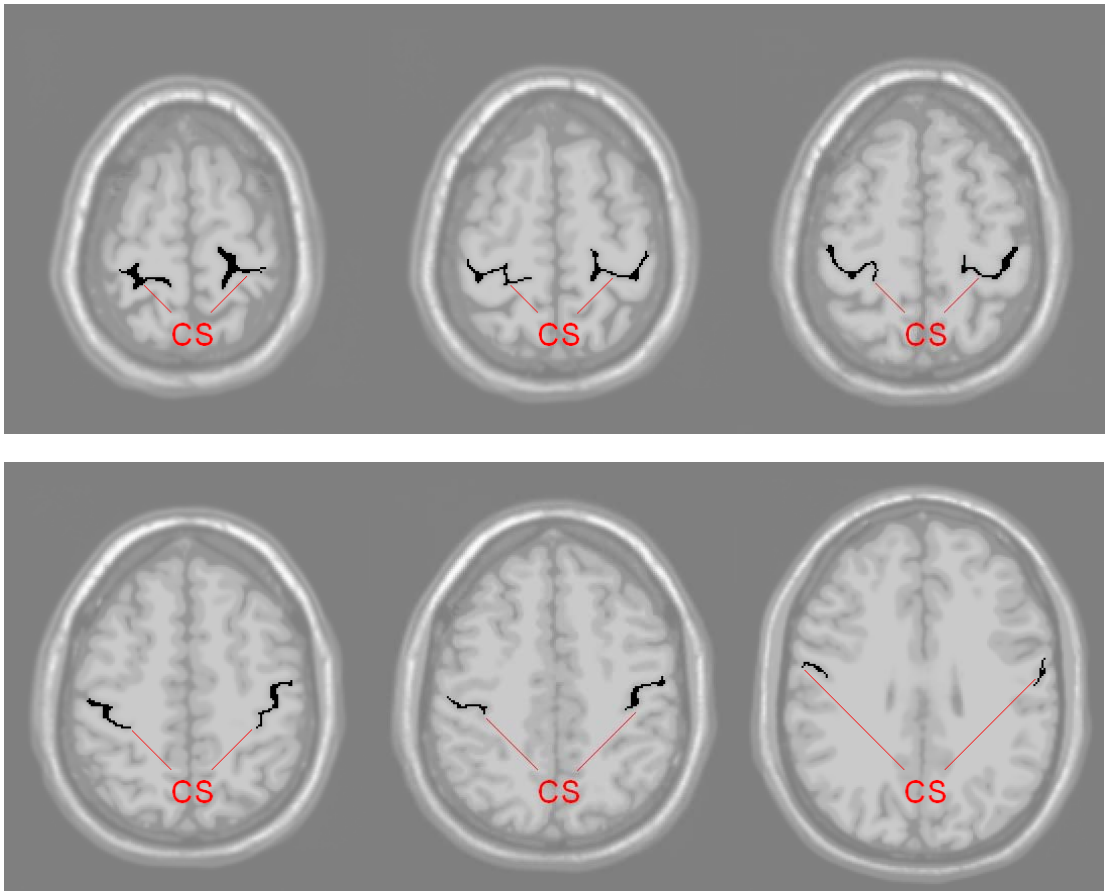

Fig 6.1 The final results of the CS identified and segmented in several axial slices.

In **Fig 6.2**, 3D renderings of the segmented CS (2 CSs from the same brain) are visualized from different view points:

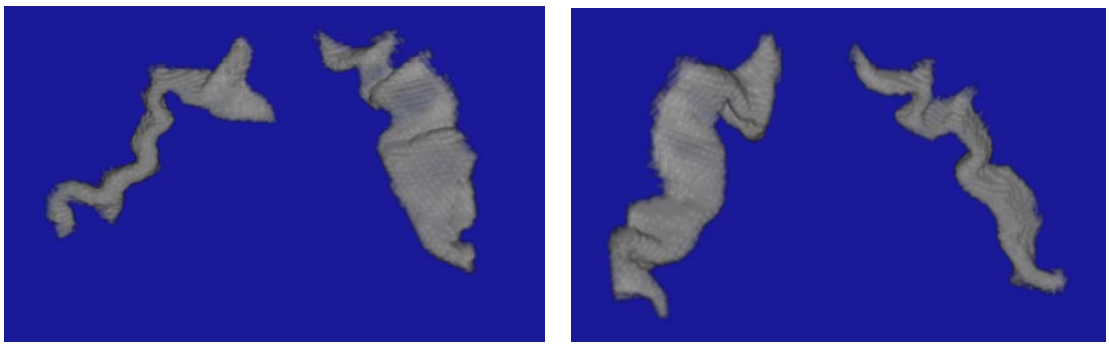

Fig 6.2 The 3D visualization of the segmented CS.

6.3 Discussion

Among the 18 phantom datasets, the CS is successfully identified and segmented from 16 datasets; the 2 failed cases are all with high noise level (9%). For the 4 patient-specific datasets, the CSs are also identified and segmented.

26 real datasets have been studied in order to get statistical anatomical knowledge, which is indispensable to determine the value of some parameters in our approach (for example α in 3.4).

The quantification work is difficult to be applied on this approach, because there is too little CSF component in the CSs in the phantom datasets (sometimes the broken part has larger volume than the connected part), while the skeletonization add many voxels which do not exist in the original MRI datasets. Thus, the quantification work will have less meaning due to this problem which is not easy to avoid.

The 3D volume of the sulci within ROI

The calculation results show that the CS has the largest 3D volume within the ROI. Take the dataset with no noise and inhomogeneity for example, the biggest 3D volume of the sulci within the ROI on the left hemisphere is 6176 mm^3 and that value on the right hemisphere is 5507 mm^3. **Table 6.1** shows the 3D volume information of the sulci within the ROI of the 4 clinical data sets (the PoCS has a little component in the ROI and is not included):

Data set number:	(1)	(2)	(3)	(4)
3D Volume of the PreCS (mm^3)	461	166	499	1497
3D Volume of the CS (mm^3)	3548	3145	3166	3020

Table 6.1 The 3D volume information of the sulci within the ROI.

Sensitivity to noise

When the noise level is smaller than 9%, it does not have any visible influence on the final result. However, when the noise level is 9%, over-segmentation occurs and the algorithm failed for the studied cases.

Sensitivity to inhomogeneity

The algorithm is quite insensitive to inhomogeneity. It can identify and segment the CS at the inhomogeneity levels of 0, 20% and 40% along with additional noise levels of 0, 1%, 3%, 5%, and 7%.

Influence of GM

GM plays a very important role in our algorithm. GM is helpful in region growing to counteract the broken sulci due to the partial volume effect. Although the GM may cause over-segmentation, its influence can be eliminated through employing the over-segmentation-removal algorithm we designed, skeletonization and 3D boundary look-up table.

Running time

For a normal 3D MR raw image data ($181 \times 217 \times 181$ for example), it takes less than 15 minutes to run the whole algorithm with a P4 2.4GHz, 768M PC.

Advantages

- fully automatic and no manual intervention is required
- using GM and skeletonization to counteract the partial volume effect and keep the connectivity of the sulci
- robust to the fair level of noise (no more than 7%) and inhomogeneity
- combine the anatomical knowledge with image processing techniques

As the algorithm is based on the combination of image processing techniques and anatomical knowledge, it may well be extended to other imaging sequences and other modalities.

Limitation

The complicated anatomy and high variability in several top axial slices of the brain tissues increases difficulty of segmentation. Our algorithm is sensitive to the high level of noise.

6.4 Conclusion

In this thesis we present a knowledge-driven method for identification and segmentation of the CS from human brain MR images through 3D region growing and calculating the volume of the sulci within the 3D region between the two coronal planes passing through the AC and PC. The experimental result shows that the sulci can be segmented through region growing of the CSF and GM to handle the partial volume effect, provided over-segmentation due to GM is removed by our proposed algorithm and 3D boundary look-up table and the unnecessary GM component is

removed by skeletonization, while minimum GM is kept to keep the connectivity of the CS. Comparing the 3D volume of the sulci in the well defined ROI proves to be an effective way to identify the CS. Experiments against 18 T1-weighted phantom datasets and 4 clinical datasets are encouraging showing that the algorithm is robust to inhomogeneity and fair noise level but sensitive to high noise level.

The CS is a structure filled with liquid, rather than a tissue. There may be no CSF component in the CS. Although the GM and the skeletonization may bring 1~2- voxel wide mistake, for MR images, the purpose of the skeleton is to connect the broken part of the sulci, not to recover the original ideal image. The importance of the skeleton is to connect the broken sulcus and indicate the location of it, since the CS is rather a structure.

6.5 Prospects

Our algorithm provides a good starting point in automatically identifying and segment the CS from MR images. There are still some spaces left to be done in the future.

The brain tissue arrangement in the top axial slices is complex. To deal well with the processing on this part will enhance the segmentation result on the whole.

This algorithm needs to be further tested against more data, especially patient cases. And it is better if this algorithm can be applied in other pulse sequence MR image (T2) and other modalities (CT).

A morphometric analysis and variability study of the CS, extension of this algorithm

to the PreCS and PoCS and extraction in the present of pathology may be another useful extension of this work. Furthermore, robustness to high level of noise is a direction to explore.

Author's Publication

[1] Wei Zuo, Qingmao Hu, Aamer Aziz, Kiafock Loe, and Wieslaw L. Nowinski. "Knowledge-driven Segmentation of the Central Sulcus from Human Brain MR Images," *Proc. IEEE International Conference of Image Processing (ICIP)*, October 24-27, 2004 Singapore.

References

[1] L.L. Altshuler, G. Bartzokis, T. Grieder, J. Curran, T. Jimenez, K. Leight, J. Wilkins, R. Gerner and J. Mintz, An MRI Study of Temporal Lobe Structures in Men with Bipolar Disorder or Schizophrenia, *Biol. Psychiatry* 48 (2000), pp. 147–162.

[2] K.J. Behnke, M.E. Rettmann, D.L. Pham, D.G. Shen, S.M. Resnick, C. Davatzikos, J. Prince, Automatic classification of sulcal regions of the human brain cortex using pattern recognition, *Proc. SPIE Int. Soc. Opt. Eng*. 5032, 1499 (2003).

[3] M.S. Berger, W.A. Cohen, and G.A. Ojemann, Correlation of Motor Cortex Brain Mapping Data with Magnetic Resonance Imaging, *J Neurosurg*, vol. 72, pp. 383-387, 1990.

[4] S. Chitoku, H. Otsubo, R.A. Sharma, E. Pang, J.T. Rutka, and O.C. Snead, Identification of the Central Selcus in Adolescents with Epilepsy: MEG Results Confirmed by Cortical Stimulation of Subdural Grid, *Proc. 12th International conference on Biomagnetism*, pp. 0451-0454, 2000.

[5] Y. Fujiki, S. Kobashi, K. Kondo, and Y. Hata, User-Guided Segmentation of the Frontal Lobe Using Fuzzy Rule-Based Active Contour Model, *Proc. 1st Int. Conf. on Soft Computing and Intelligent Systems*, 2002.

[6] M. Gado, J. Hanaway, and R. Frank, Functional Anatomy of the Cerebral Cortex by Computed Tomography, *J Computer Assist Tomogr*, vol. 3, pp. 1-19, 1979.

[7] G.L. Goualher, E. Pricky, D.L. Collins, R. Venugopal, C. Barillot, and A.C. Evans, Automated Extraction and Variability Analysis of Sulcal Neuroanatomy, *IEEE Trans. Med. Imag*., vol. 18, pp. 206-217, Mar. 1998.

[8] P. Hauser, J. Matochik, L.L. Altshuler, K.D. Denicoff, A. Conrad, L. Ximing and R.M. Post, MRI-Based Measurements of Temporal Lobe and Ventricular Structures in Patients with Bipolar I and Bipolar II Disorders. *J. Affect. Disord.* **60** (2000), pp. 25–32.

[9] C.J. Hilditch, Linear Skeletons from Square Cipboards, *Machine Intelligence*, vol.4, pp. 402-420, 1969.

[10] Q.M. Hu, U. Langlotz, J. Lawrence, F. Langlotz, and L.P. Nolte, A Fast Impingement Detection Algorithm for Computer-Aided Orthopedic Surgery, *Computer Aided Surgery*, vol. 6, pp.104-110,2001.

[11] Q.M Hu, W.L. Nowinski, A Rapid Algorithm for Robust and Automatic Extraction of the Midsagittal Plane from Neuroimages Based on Local Symmetry and Outlier Removal, *NeuroImage*, vol. 20, pp. 2153-2165, 2003.

[12] Q.M. Hu, W.L. Nowinski, Knowledge Driven Extraction of the Four Modified Talairach Cortical Landmarks (A, P, L, and R) from MR Neuroimages, *Fourth IEEE Symposium on Bioinformatics and Bioengineering BIB*E, pp. 93-99, 2003.

[13] T. Inoue, H. Shimizu, N. Nakasato, T. Kumabe, and T. Yashimoto, Accuracy and Limitation of Functional Magnetic Resonance Imaging for Identification of the Central Sulcus: Comparison with Magnetoencephalography in Patients with

Brain Tumors, *NeuroImage*, vol. 10, pp. 738-748, 1999.

[14] S. Iwasaki, H. Nakagawa, A. Fukusumi, K. Kichikawa, K. Kitamura, H. Otsuji, H. Uchida, H. Ohishi, K. Yaguchi, H. Sumie, and Y. Kuru, Identification of Pre- and Post-Central Gyri on CT and MR Images on the Basis of the Medullary Pattern of Cerebral White Matter, *Radiology*, vol. 179, pp. 207-213, 1991.

[15] D.K. Kido, M.L. May, A.W. Levinson, and W.E. Benson, Computed Tomographic Localization of the Precentral Gyrus, *Radiology*, vol. 135, pp. 373-377, 1980.

[16] C.L. Li, D.B. Goldgof, and L.O. Hall, Knowledge-Based Classification and Tissue Labeling of MR Image of Human Brain, *IEEE Trans. Medical Imaging*, vol. 12, no. 4, pp. 740-750, 1993.

[17] G. Lohmann, Extracting Line Representations of Sulcal and Gyral Patterns in MR Images of the Human Brain, *IEEE Trans. Medical Imaging*, vol. 17, pp. 1040-1048, Dec. 1998.

[18] G. Lohmann, D.Y. Cramon, Automatic Labeling of the Human Cortical Surface Using Sulcal Basin, *Medical Image Analysis*, vol. 4, pp. 179-188, 2000.

[19] T. Matsui, The Basis of CT Diagnosis: Normal Brain Anatomy for CT Diagnosis, *Neurol Med Chir*, vol. 20, pp. 971-981, 1980.

[20] T.P. Naidich, MR Imaging of Brain Surface Anatomy, *Neuroradiology*, vol. 33 (Suppl), pp. S95-S99, 1991.

[21] T.P. Naidich, T.C. Brightbill, The Pars Marginalis, II: the Pars Deflection

Sign, a White Matter Pattern for Identifying the Pars Marginalis in Axial Plane CT and MRI, *Int. J. Neuroradiol*, vol. 2, pp. 20-24, 1996.

[22] W.L. Nowinski, and A. Thirunavuukarasuu, Methods and Apparatus for Processing Medical Images, PCT patent application, PCT/SG00/00185, 2002.

[23] M. Ono, S. Kubik and C.D. Abernathey, Atlas of the Cerebral Sulci, Thieme, Stuttgart. New York, 1990.

[24] N. Otsu, A Threshold Selection Method from Gray-Level Histograms, *IEEE Trans. Syst., Man, Cybern.*, vol. SMC-9, no. 1, pp.62-66, Jan. 1979.

[25] G. Ruggiero, EncephalographyToday, *Acta Radiol Suppl*, vol. 5, pp. 705-715, 1966.

[26] S. Sandor, and R. Leahy, Surface-Based Labeling of Cortical Anatomy Using a Deformable Atlas, *IEEE Trans. Medical Imaging*, vol. 16, pp. 41-54, Feb. 1997.

[27] Z.Y. Shan, G.H. Yue, and J.Z. Liu, Automated Histogram-Based Brain Ssegmentation in T1-Weighted Three-Dimensional Magnetic Resonance Head Images, *NeuroImage*; vol. 17, pp. 1587-1598, 2002

[28] D.F. Sobel, CC. Gallen, BJ. Schwarts, TA. Waltz, B. Copeland, S. Yamada, EC. Hirschkoff, and FE. Bloom, Locating the Central Sulcus: Comparison of MR Anatomic and Magnetoencephalographic Functional Methods, *AJNR: Am J Neuroradiol*; vol. 14, pp. 915-925, 1993.

[29] J. Talairach, and P. Tournoux, Co-planar Stereotaxic Atlas of the Atlas of the Human Brain, Thieme, Stuttgart. New York, 1988.

[30] Y. Xia, Q.M. Hu, A. Aziz, and W.L. Nowinski, A Knowledge-Driven

Algorithm for a Rapid and Automatic Extraction of the Human Cerebral Ventricular System from MR Neuroimages, *NeuroImage*; vol. 21, pp. 269-282, 2004

[31] http://www.mghneuroradiology.org/Petitte_Presentation/Petitti-.ppt